IMPERIAL COLLEGE LONDON

ALBERT-LUDWIGS-UNIVERSITÄT FREIBURG

MSCI THESIS

Efficient Quantum Transport in Disordered Networks with Vibrations

---

Hlér Kristjánsson

Supervisor: Andreas Buchleitner
Co-supervisors: Gabriel Dufour
Christian Scheppach

4th July 2017

Abstract

The potential role of quantum coherence in the fast and efficient energy transport observed in light-harvesting complexes of photosynthetic organisms has been a topic of extensive research in recent years. In these systems, an excitation is conveyed by a small number of dipole-coupled molecules which form a network. Such networks exhibit statistical variations from one realisation to another, as well as fluctuations due to coupling with their environment. This motivates the search for structural design principles of the networks that ensure good transport despite this variability. Walschaers *et al.* [1] proposed a model for efficient quantum transport across disordered networks relying on *centrosymmetry* of the network and a *dominant doublet* spectral structure. Here, this model is extended to take into account large energy differences between the sites of the network as well as an explicit time-dependence due to coupling to a vibrational mode. With the aid of Floquet theory, symmetries of the network in space as well as in time are considered. Analytical calculations, along with numerical simulations, result in the proposal of the generalised design principles *Floquet-antisymmetry* and *dominant Floquet doublet*, which are shown to lead to fast and efficient vibrationally-assisted quantum transport.

Zusammenfassung

Die mögliche Rolle von Quantenkohärenz beim schnellen und effizienten Energietransport in Lichtsammelkomplexen von photosynthetischen Organismen war in den letzten Jahren ein aktives Forschungsgebiet. In diesen Systemen wird eine Anregung durch einige dipolgekoppelte Moleküle transportiert, die ein Netzwerk bilden. Solche Netzwerke sind statistisch variabel von Realisierung zu Realisierung, und sie unterliegen Fluktuationen aufgrund der Kopplung an die Umgebung. Dies motiviert die Suche nach strukturellen Merkmalen solcher Netzwerke, welche trotz dieser Variabilität guten Transport gewährleisten. Walschaers *et al.* [1] schlugen ein Modell effizienten Quantentransports durch ungeordnete Netzwerke vor, das auf der *Zentrosymmetrie* des Netzwerks und dem Vorliegen eines *dominanten Doublets* in seinem Spektrum beruht. In der vorliegenden Arbeit wird das Modell dahingehend erweitert, dass u. U. große Energieunterschiede zwischen den Knoten des Netzwerks sowie eine explizite Zeitabhängigkeit aufgrund der Kopplung an eine Schwingungsmode berücksichtigt werden. Mithilfe der Floquettheorie werden verallgemeinerte Netzwerksymmetrien in Raum *und* Zeit ausgenützt und entsprechend neue Designprinzipien – *Floquet-Antisymmetrie* und *dominantes Floquet-Doublet* – vorgeschlagen. Analytische Rechnungen und numerische Simulationen zeigen, dass diese neuen Konstruktionsprinzipien schnellen und effizienten Quantentransport gewährleisten.

Contents

Preface

The work presented in this thesis is the result of an MSci research project carried out in the Quantum Optics and Statistics group, led by Professor Andreas Buchleitner, at the University of Freiburg. The project directly follows on from previous work in the group, by Mattia Walschaers during his PhD [1–3] and Jonathan Brugger during his BSc thesis [4]. The former laid the foundations for the overall aim of all three projects, namely finding *design principles* for efficient quantum transport in disordered networks. The initial inspiration for this work was energy transport in biological networks, such as the FMO photosynthetic complex [5]. Two simple design principles were found to greatly increase the transport efficiency through static disordered quantum networks. The latter project then followed on with an investigation into networks with large on-site energy differences under periodic driving. The current thesis continues this investigation and presents a generalisation of the two aforementioned design principles to the time-dependent network.

The project was carried out independently and supervised by two post-doctoral researchers in the group, Gabriel Dufour and Christian Scheppach, in addition to the group leader Andreas Buchleitner. The calculations presented in the Results chapter of the thesis are original work unless otherwise stated. The application of Floquet theory and perturbation theory calculations to time-periodic Hamiltonians is based on the work of Shirley [6] and was implemented for a 2×2 Hamiltonian in the context of quantum transport by Jonathan Brugger [4]. In the current thesis, the application is extended to 3×3 Hamiltonians, which is only feasible in the presence of specific symmetries. *Floquet-antisymmetry* and its proposal as a design principle is a completely original idea, and was also used to facilitate the perturbation theory calculations. The formulation of the *dominant Floquet doublet* design principle is a generalisation of a condition with the same name albeit valid only in a special case, presented in [4]. Some elements of the formulation of the generalised condition and associated calculations are based on (unpublished) ideas from Jonathan Brugger [7]. The investigation into statistics of transfer times is similarly a generalisation of the results presented in [4]. All computer programs used for analytic calculations and numerical simulations (written in *Mathematica* and *Python*) are original.

Chapter I

Introduction

The potential role of quantum mechanical effects on the functionality of biological systems has been a fiercely debated topic in the last decade. Traditionally, it was assumed that quantum coherences cannot be sustained at ambient temperatures, rendering them irrelevant in biological processes. However, in 2007, Engel *et al.* found experimental evidence for remarkably long-lived quantum coherences in the Fenna-Matthews-Olson (FMO) light-harvesting complex [5]. The FMO complex is a protein matrix containing of several chlorophyll molecules, which serves as a 'wire' for energy transport between the light-capturing antenna and reaction centre in green sulphur bacteria [8]. These photosynthetic bacteria live in very low-light conditions, requiring highly efficient mechanisms for both capturing the limited number of photons that come their way and transporting the harvested energy to the reaction centre, where it is converted to chemical energy that can be used by the organism. Evidence suggests that their quantum efficiency of energy transport, i.e. the fraction of electromagnetic energy collected by the antenna eventually used for chemical reactions, is close to 100% [8]. The spectroscopic data in [5] further suggested that this high efficiency is a result of the reported quantum coherences. This sparked the yet unresolved debate on whether quantum coherences play a non-trivial role in biological systems [9, 10], for which the FMO complex is a prime contender.

A variety of experimental and theoretical work has been conducted on potential quantum effects in the FMO complex. Two-dimensional electronic spectroscopy has been an important experimental tool to probe the dynamics of the system. The initial reports claimed that the energy from each photon is transported through the FMO wire with non-vanishing electronic coherences between the chlorophyll molecules during transport [5]. Recent findings suggest that these electronic degrees of freedom are coupled to vibrational degrees of freedom in the system [11]. Nevertheless, not all experiments agree and some have argued that long-lived quantum coherences do not play a role in photosynthetic energy transfer [12]. Computational models have also made a significant contribution to the debate, where detailed simulations of the FMO complex have been created to study population dynamics of the molecular sites.

Such models have been created both with and without explicit quantum coherences present. Ishizaki and Fleming found that quantum coherences are indeed likely to aid energy transport [13], while others have argued that any improvements in efficiency of a quantum coherent model compared to a classical one are minimal [14]. Thus the question of whether quantum coherences have a *functional* effect on biological energy transport remains an open question.

One theoretical approach to contribute to this debate was presented by Walschaers *et al.* [1–3], which emphasises the statistical variability present in biological systems. In practice, the structure of each realisation of the FMO complex exhibits microscopic *disorder* variations from a general common architecture. Furthermore, each realisation may exhibit time-dependent variations due to vibrations in the protein structure. Experimental results, showing that the efficiency of transport is close to 100%, correspond to an ensemble average over many such microscopic realisations. This motivates a search for *design principles* that can be imposed on the structure of the FMO complex to guarantee efficient transport, in a way that is robust against statistical variations [2, 3]. Explicitly taking a quantum mechanical model, the design principles must also ensure that the transport occurs on timescales faster than typical decoherence timescales such that quantum coherences are maintained; coherences have been shown to last up to 660 fs in experiment [5].

Walschaers *et al.* proposed a model of quantum coherent energy transport in the FMO complex describing the dominant physical processes, with statistical disorder at its core [1]. The FMO complex was modelled as a network of two-level systems corresponding to the chlorophyll molecules, with dipole-dipole couplings between one another. The couplings between the sites and their respective energy splittings were initially taken to be random variables. Walschaers *et al.* studied the propagation of an excitation initially carried by a single 'input' molecule across such a network. Then, design principles were sought, which enhance the probability of achieving efficient transport to a given 'output' molecule. Two such design principles were found, namely *centrosymmetry* and the *dominant doublet* (which will be defined in § II.3.1). The statistical structure and generality of this model enables it to have potential applications in many other fields. Indeed, achieving efficient transport in quantum networks subject to disorder variations is of paramount importance in a variety of areas, ranging from solar-cell design to quantum information [1].

The aim of this thesis is to generalise the statistical model of efficient quantum transport in disordered networks presented in [1], to allow for two additional features that are present in realistic networks. First, the energy splittings of the molecules are considered independently from the random distribution of the inter-site couplings. Following experimental measurements of these energies in the FMO complex, they are taken to follow an energy gradient, where the value of the energy splitting at each site gradually decreases from the input to the output site [15]. Secondly, coupling of the network to its environment is explicitly considered. The FMO network is embedded in a complex biological superstructure and is therefore affected by

the various vibrational degrees of freedom present in the superstructure. Keeping with the minimalistic structure of the model, coupling of the electronic degrees of freedom to a single-frequency vibrational mode is considered, by introducing an additional set of time-periodic couplings between the sites. Various investigations of this extended model were conducted in [4]. The present thesis aims to consolidate these investigations and to formulate concrete design principles, analogous to those found for the simpler static case, for fast and efficient energy transport in the more general quantum model.

The thesis will proceed as follows. First, a theoretical description of the quantum network model is given, followed by a summary of the main theoretical methods used. An outline of the previous results concerning both the initial and extended models is given, concluding with three concrete open problems which are set out to be answered in the thesis. The Results section goes through these open problems in turn, beginning with a discussion of symmetries present in the system. This leads to the formulation of a design principle analogous to the previous *centrosymmetry*, namely *Floquet antisymmetry*, which is shown to statistically increase the probability of obtaining efficient transport. Transport under a three-site system exhibiting such a symmetry is analytically calculated. The characteristics of this system which are responsible for efficient transport are then used to formulate a second design principle for general N-site systems. This second design principle is called the *dominant Floquet doublet*, analogously to the *dominant doublet* from the original model, and is shown to guarantee efficient transport. In addition, a short investigation on the statistics of the *speed* of transport between the input and output sites is presented. The results are then discussed and compared to the those of the original model. Finally, applications to the FMO complex and other fields are discussed, accompanied by an outlook for further research.

Chapter II

Theoretical Framework

This chapter begins by outlining the theoretical model of the quantum networks studied in this thesis and in previous work. Two of the main theoretical methods required for both earlier and present results are then presented, namely Floquet theory and a suited perturbation theory. The chapter concludes with a summary of previous results and a discussion of open questions.

II.1 Quantum network model

In this work, energy transport through a quantum network of N sites is investigated, with an initial excitation localised at the input site and propagating through the network to the output site. The FMO complex is modelled as such a network, with the input and output sites connected to the antenna complex and reaction centre, respectively. Here, only energy transport through the wire itself is considered and the effects of coupling to the antenna and reaction centre [3], which are beyond the scope of this thesis, are neglected.

The sites correspond to the chlorophyll molecules [8] of the FMO complex and each site n is modelled as a two-level system with energy splitting (on-site energy) V_{nn}. Furthermore, the sites are taken to be coupled via the dipole-dipole interaction, with (real) couplings $V_{nm} = V_{mn}$ between sites n and m. The system is formulated quantum mechanically by defining site basis vectors $|n\rangle$ with $n \in \{1,\ldots,N\}$, each corresponding to an excitation localised at site n, which span the N-dimensional single-excitation Hilbert space $\mathscr{H} = \mathbb{C}^N$. For the simplest version of the model, a Hamiltonian for the system can be written down as

$$H_0 = \sum_{n,m=1}^{N} V_{nm} |n\rangle \langle m|, \tag{II.1}$$

with the diagonal elements of the Hamiltonian corresponding to the on-site energies and the off-diagonal elements corresponding to the couplings between the sites [3]. The FMO complex has seven or potentially eight sites [8, 15]. For the sake of generality, a general network of N

sites with N of the order of ten is considered.

The electronic state of the system at time t is given by $|\psi(t)\rangle \in \mathscr{H}$, where $|\psi(t)\rangle$ can be expanded in terms of the site basis vectors, with expansion coefficients $c_n(t)$, as

$$|\psi(t)\rangle = \sum_{n=1}^{N} c_n(t)\,|n\rangle\,, \tag{II.2}$$

where $|c_n(t)|^2$ gives the probability at time t of finding the excitation localised at site n. The initial state of the system is taken to be $|\psi(t=t_0)\rangle = |\text{in}\rangle$, where $|\text{in}\rangle = |1\rangle$ in the site basis, i.e. the system starts with an excitation localised at the input site. The initial input time t_0 of the excitation into the system is, for now, set to zero without loss of generality. The system is then taken to evolve unitarily under the network Hamiltonian H_0, with the state of the system at time t given by $|\psi(t)\rangle = e^{-iHt}\,|\psi(0)\rangle$, where the phase angle is measured in units of $\hbar$. The *transfer probability*, i.e. the probability of the excitation being localised at the output site $|\text{out}\rangle = |N\rangle$ at time t, is given by

$$\mathscr{P}(t) \coloneqq |\,\langle \text{out}|\psi(t)\rangle\,|^2. \tag{II.3}$$

The quantity of interest is the maximum value of this transfer probability, and the time at which the maximum is reached. If this probability is close to one, then the quantum efficiency [8] is said to be high. This corresponds to every excitation coming into the network also coming out at the other end, which is what bacteria living in low-light conditions require to make use of every photon that comes their way. Furthermore, the transport is required to occur at timescales shorter than the typical time for decoherence to significantly affect the transport. Therefore, a reference time T_R is chosen, within which the maximum of $\mathscr{P}(t)$ is required to occur. Thus, the figure of merit is chosen to be the maximum transfer probability in an interval of length T_R:

$$\mathscr{P}_\text{max} \coloneqq \max_{t\in[0,T_\text{R})} \underbrace{|\,\langle \text{out}|\psi(t)\rangle\,|^2}_{=\mathscr{P}(t)}, \tag{II.4}$$

with $\mathscr{P}_\text{max} \approx 1$ corresponding to both *fast* and *efficient* transport, assuming a sufficiently short T_R. The time at which this maximum (first) occurs is called the transfer time, τ.

The statistical disorder eminent in biological systems [2] is incorporated by letting the Hamiltonian matrix elements be random variables, with each realisation of the FMO network exhibiting statistical variations from every other. Following [1], the matrix elements are sampled from a Gaussian Orthogonal Ensemble (GOE), such that

$$V_{nm} \sim \begin{cases} \mathscr{N}(0, 2\xi^2) & \text{for } n = m \\ \mathscr{N}(0, \xi^2) & \text{for } n \neq m \end{cases}, \tag{II.5}$$

where $\mathscr{N}$ is the normal distribution, with zero mean and variances $2\xi^2$ and ξ^2, respectively. The factor of 2 for $n = m$ is a result from random matrix theory, arising from the hermiticity of

the Hamiltonian [3].

Comparing the Hamiltonian of Eq. (II.1) to an ensemble averaged Hamiltonian inferred from experimental and computational data (see [3,15]), it can be seen that the literature Hamiltonian exhibits diagonal elements with a descending trend from the input to the output site, with V_{11} between 5 and 300 times larger than the size of the various coupling elements, and $V_{NN} = 0$. This suggests that for a more realistic model of the FMO complex, an additional term needs to be added to the Hamiltonian, describing the larger on-site energies with a descending trend. For statistical purposes, the model is extended to consider new on-site energy terms $D_n,\ n \in \{1,\ldots,N\}$, with

$$D_n \sim \mathcal{N}\left(D_0 \frac{N-n}{N-1} - \frac{D_0}{2},\ \eta^2\right), \tag{II.6}$$

where the general descending trend is respected whilst allowing for local variations of the order of η. D_0 is a positive constant set to the order of around 10ξ [4], ensuring that the difference between the input and output on-site energies are on average an order of magnitude larger than the off-diagonal coupling elements of the Hamiltonian. The on-site energies are only defined up to a global constant. Here they have been defined such that the input and output sites have on average equal and opposite energies, for reasons of symmetry which will become clear later.

With the addition of the on-site energy terms D_n, which define a non-trivial *energy landscape*, a problem due to the conservation of energy is encountered. With the input and output sites having radically different on-site energies in comparison to the couplings, the conservation of energy forbids perfect transport between the input and output sites and makes transport ever more unlikely the greater the in-out energy difference is [3]. Therefore, an additional mechanism is required to bridge the energy gap. Experimental results, see e.g. [16], suggest that the network is coupled to vibrational degrees of freedom of the structure in which it is embedded. For a complex biological system, a multitude of vibrational modes is expected to be present, but those modes which are in near-resonance with the energy differences between the electronic states of the network are assumed to play a prominent role within the timescales considered. In keeping with the minimalistic design of the model, a second additional term of vibrational couplings $W_{nm}\cos(\omega t - \delta)$ is introduced to the Hamiltonian, corresponding to a sinusoidal oscillation of both the on-site energies and inter-site couplings, with a frequency ω representing the dominant vibrational mode. δ is an arbitrary initial phase.

Combining the energy landscape and vibrational couplings with the original Hamiltonian H_0 of Eq. (II.1), the full Hamiltonian is

$$H(t) = \underbrace{\underbrace{\sum_{n=1}^{N} D_n |n\rangle\langle n|}_{=:H_\mathrm{D}} + \underbrace{\sum_{n,m=1}^{N} V_{nm} |n\rangle\langle m|}_{=:H_0}}_{=:H_\mathrm{static}} + \cos(\omega t - \delta) \underbrace{\sum_{n,m=1}^{N} W_{nm} |n\rangle\langle m|}_{=:H_\mathrm{vib}}, \tag{II.7}$$

where the three terms of the Hamiltonian are defined as H_{D}, H_0 and H_{vib}, respectively, with $(H_{\mathrm{D}}+H_0)$ also referred to as H_{static}. Note that the original on-site energies from H_0 are explicitly kept as a part of H_0 and separate from the larger on-site energies in H_{D}. The reason for this is to retain the random matrix structure for both H_0 and H_{vib}. However, this is equivalent to absorbing both sets of on-site energies into one term, with a different standard deviation. Just as for the static couplings in H_0, the amplitudes of the vibrational couplings are taken to be distributed according to a GOE:

$$W_{nm} \sim \begin{cases} \mathcal{N}(0, 2\sigma^2) & \text{for } n = m \\ \mathcal{N}(0, \sigma^2) & \text{for } n \neq m \end{cases} . \tag{II.8}$$

It is assumed that $\sigma \ll \xi$ such that the transport is not completely dominated by the vibrations.

A final point to note is that for the time-periodic Hamiltonian, given that the Hamiltonian takes a different form at each point in time within a time period, the initial input time of the excitation into the system t_0 can no longer be chosen as zero without loss of generality. Therefore, the initial condition of the system is taken to be $|\psi(t=t_0)\rangle = |\mathrm{in}\rangle$, with the state of the system at time t and the (maximum) transfer probability also dependent on t_0:

$$\mathscr{P}_{\max}(t_0) := \max_{t\in[t_0, t_0+T_{\mathrm{R}})} \underbrace{|\langle out|\psi(t,t_0)\rangle|^2}_{=:\mathscr{P}(t,t_0)}. \tag{II.9}$$

With the model set in place, *design principles* imposed as additional constraints on the statistics to enhance the transport efficiency can be found. Before summarising the key results that have already been found to this end, the main theoretical methods required are presented.

II.2 Methods

II.2.1 Floquet theory

For a closed quantum system described by a time-dependent Hamiltonian $H(t)$, the state $|\psi(t)\rangle$ of the system evolves under the Schrödinger equation

$$i\partial_t |\psi(t)\rangle = H(t)|\psi(t)\rangle\,, \tag{II.10}$$

where $\hbar$ is set to 1 throughout this thesis. $|\psi(t)\rangle \in \mathscr{H}$, where $\mathscr{H}$ is a Hilbert space, and $H(t)$ is a Hermitian operator on $\mathscr{H}$.

Floquet theory provides a method of solving the Schrödinger equation for a time-periodic Hamiltonian analogous to the standard solution for a time-independent (static) Hamiltonian [17, 18]. Let us begin by reviewing the results for the static case before formulating the Floquet analogy for the time-periodic case.

II.2.1.a Time-independent Hamiltonian

For a Hamiltonian H constant in time on an N-dimensional Hilbert space $\mathscr{H} = \mathbb{C}^N$, the solution to the Schrödinger equation can be expressed as a linear superposition of the eigenstates $|\varphi_i\rangle \in \mathscr{H}$ of H (with corresponding eigenvalues E_i):

$$|\psi(t)\rangle = \sum_{i=1}^{N} e^{-iE_i t} a_i |\varphi_i\rangle . \tag{II.11}$$

t_0 is an initial time where the initial state is specified and the expansion coefficients a_i are determined by the initial condition $a_i = e^{iE_i t_0} \langle\varphi_i|\psi(t_0)\rangle$. The eigenstates form a complete orthonormal basis in $\mathscr{H}$:

$$\langle\varphi_i|\varphi_j\rangle = \delta_{ij}, \quad \sum_{i=1}^{N} |\varphi_i\rangle \langle\varphi_i| = \mathbb{1}_N, \tag{II.12}$$

where $\mathbb{1}_N$ is the identity operator on $\mathscr{H}$ [18].

II.2.1.b Time-periodic Hamiltonian

For a Hamiltonian $H(t)$ periodic in time with period $T = 2\pi/\omega$, i.e.

$$H(t) = H(t+T), \ \forall t \in \mathbb{R}, \tag{II.13}$$

on an N-dimensional discrete Hilbert space $\mathscr{H} = \mathbb{C}^N$, the Schrödinger equation (Eq. (II.10)) becomes a first-order linear differential equation with periodic coefficients. This enables the use of the Floquet theorem, which states that the solution of the equation can be expressed as a linear superposition of the *Floquet states* $|\phi_i(t)\rangle$ of $H(t)$:

$$|\psi(t)\rangle = \sum_{i=1}^{N} e^{-i\varepsilon_i t} a_i |\phi_i(t)\rangle , \tag{II.14}$$

where $\varepsilon_i \in \mathbb{R}$ are known as *quasi-energies* and the a_i are time-independent expansion coefficients given at an initial time t_0. The Floquet states are also T-periodic:

$$|\phi_i(t)\rangle = |\phi_i(t+T)\rangle , \ \forall t \in \mathbb{R}. \tag{II.15}$$

By inserting the solution of Eq. (II.14) back into Eq. (II.10), it can be seen that the Floquet states and quasi-energies are in fact eigenvectors and eigenvalues of the *Floquet Hamiltonian* $[H(t) - i\partial_t]$ such that

$$[H(t) - i\partial_t]|\phi_i(t)\rangle = \varepsilon_i |\phi_i(t)\rangle . \tag{II.16}$$

It can be seen that the Floquet states and quasi-energies are not uniquely defined [18]. For each Floquet state $|\phi_i(t)\rangle$ and corresponding quasi-energy ε_i, there exist an infinite number of

equivalent Floquet states and quasi-energies

$$|\phi_{i,p}(t)\rangle = e^{ip\omega t}\,|\phi_i(t)\rangle\,,\ \varepsilon_{i,p} = \varepsilon_i + p\omega, \tag{II.17}$$

for any $p \in \mathbb{Z}$. This equivalence can be understood by noting that the combination of $|\phi_{i,p}(t)\rangle$ and $\varepsilon_{i,p}$ constitutes the same Floquet expansion as the combination of $|\phi_i(t)\rangle$ and ε_i when inserted into Eq. (II.14):

$$e^{-i\varepsilon_{i,p}t}\,|\phi_{i,p}(t)\rangle = e^{-i(\varepsilon_i+p\omega)t}e^{ip\omega t}\,|\phi_i(t)\rangle = e^{-i\varepsilon_i t}\,|\phi_i(t)\rangle\,. \tag{II.18}$$

Thus, the quasi-energy spectrum is ω-periodic. The Floquet periodicity can be expressed in terms of equivalence classes

$$\{p \in \mathbb{Z} : (|\phi_{i,p}(t)\rangle\,, \varepsilon_{i,p})\} \tag{II.19}$$

of equivalent pairs of Floquet states and quasi-energies. Given that each quasi-energy interval of size ω contains exactly one member of each class of equivalent quasi-energies, a choice can be made to consider only quasi-energies in the first *Floquet zone*: $[-\omega/2, \omega/2)$, and their corresponding Floquet states. This removes the ambiguity in the definition of the Floquet states. Furthermore, restriction to the first Floquet zone means that the number of Floquet states equals the number of dimensions N of $\mathbb{C}^N = \mathscr{H}$. Hence, it can be shown that the Floquet states in the first Floquet zone form a complete orthonormal basis in $\mathscr{H}$ *at all times* t [19, 20]:

$$\langle\phi_i(t)|\phi_j(t)\rangle = \delta_{ij},\quad \sum_{i=1}^{N} |\phi_i(t)\rangle\,\langle\phi_i(t)| = \mathbb{1}_N,\quad \forall t. \tag{II.20}$$

The orthonormality relation implies that the expansion coefficients are given by

$$a_i = e^{i\varepsilon_i t_0}\,\langle\phi_i(t_0)|\psi(t_0)\rangle\,. \tag{II.21}$$

Here, the analogy with the static case can be seen: the Floquet expansion of Eq. (II.14) together with the orthonormality and completeness conditions of Eq. (II.20) are analogous to the static expansion of Eq. (II.11) with the orthonormality and completeness conditions of Eq. (II.12) [18].

Returning to Eq. (II.16), this time-dependent (specifically: time-periodic) problem on $\mathscr{H} = \mathbb{C}^N$ can be viewed as an eigenvalue problem in the composite *Floquet Hilbert space*

$$\mathscr{H}_{\mathrm{F}} := \mathbb{C}^N \otimes \mathrm{L}^2\big([0,T)\big), \tag{II.22}$$

where $\mathrm{L}^2([0,T))$ is the (infinite-dimensional) Hilbert space of all T-periodic square-integrable functions. In this interpretation, the periodic time-dependence of the Floquet states in $\mathbb{C}^N$ should be considered as functions in the Hilbert space $\mathrm{L}^2([0,T))$. Formally, this enables abstract Floquet states $||\phi_i\rangle\rangle \in \mathscr{H}_{\mathrm{F}}$ to be written down, in which the time-dependence is completely

absorbed into the structure of the Hilbert space and no longer explicit in the states. This means that the full time evolution of the $|\phi_i(t)\rangle$ over $[0,T)$ is contained in $||\phi_i\rangle\rangle$. Now, an abstract Floquet Hamiltonian H_F can be defined as an operator on $\mathscr{H}_\mathrm{F}$, representing $[H(t)-i\partial_t]$ over a whole time period [18]. This leads to the abstract Floquet eigenvalue equation

$$H_\mathrm{F}\,||\phi_i\rangle\rangle = \varepsilon_i\,||\phi_i\rangle\rangle\,, \tag{II.23}$$

which is equivalent to Eq. (II.16).

To understand the structure of the composite Hilbert space $\mathscr{H}_\mathrm{F}$, let us begin by writing down a general state in each of the two constituent Hilbert spaces, $|\psi\rangle \in \mathbb{C}^N$ and $|\Psi\rangle \in \mathrm{L}^2\big([0,T)\big)$ [21,22]. This gives

$$|\psi\rangle = \sum_{n=1}^{N} c_n\,|n\rangle\,, \tag{II.24}$$

$$|\Psi\rangle = \int_0^T \mathrm{d}t\; C(t)\,|t\rangle\,, \tag{II.25}$$

where the $|t\rangle\,, t\in[0,T)$, form a continous basis in $\mathrm{L}^2\big([0,T)\big)$, with the probability of the state being localised at time t given by the coefficient functions $|C(t)|^2 = |\,\langle t|\Psi\rangle\,|^2$ (in analogy to the $|x\rangle$ states for a continous spatial degree of freedom [21]). In other words, $|t\rangle$ corresponds to a delta function at time t. A Floquet state in the composite space, $||\phi_i\rangle\rangle \in \mathscr{H}_\mathrm{F}$, can thus be expanded as a tensor product of the two constituent expansions as

$$||\phi_i\rangle\rangle = \sum_{n=1}^{N}\int_0^T \mathrm{d}t\;\phi_i^n(t)\,|n\rangle\otimes|t\rangle\,, \tag{II.26}$$

where $\phi_i^n(t)$ are coefficient functions with both a discrete n index and a continuous t dependence [18,19]. Given a state $||\phi_i\rangle\rangle \in \mathscr{H}_\mathrm{F}$, the corresponding state $|\phi_i(t)\rangle$ is given by

$$|\phi_i(t)\rangle = \sum_{n=1}^{N}\phi_i^n(t)\,|n\rangle\,. \tag{II.27}$$

In the following, $|\phi_i(t)\rangle$, seen as a *function* of time, will be considered a member of $\mathscr{H}_\mathrm{F}$, while at *each point in time* it is a member of $\mathscr{H}$.

The inner product on $\mathrm{L}^2\big([0,T)\big)$ is defined by

$$\langle\Psi_1|\Psi_2\rangle = \frac{1}{T}\int_0^T \mathrm{d}t\; C_1^*(t)C_2(t). \tag{II.28}$$

Thus, the inner product between two Floquet states on $\mathscr{H}_\mathrm{F}$ is

$$\langle\langle\phi_i||\phi_j\rangle\rangle = \frac{1}{T}\int_0^T \mathrm{d}t\,\langle\phi_i(t)|\phi_j(t)\rangle = \delta_{ij}, \tag{II.29}$$

where the Floquet states in $\mathscr{H}_\mathrm{F}$ form an orthonormal basis [19].

II.2.1.c Determination of Floquet states and quasi-energies

The standard method for calculating the Floquet states of a given Hamiltonian $H(t)$, i.e. solving Eq. (II.16), is by Fourier transformation to the frequency domain and diagonalisation of the resulting Fourier-transformed Hamiltonian [18]. The Fourier expansions of $|\phi_i(t)\rangle$ and $H(t)$ are given by

$$|\phi_i(t)\rangle = \sum_{k\in\mathbb{Z}} |\tilde{\phi}_i(k)\rangle\, e^{ik\omega t}, \text{ where } |\tilde{\phi}_i(k)\rangle = \frac{1}{T}\int_0^T \mathrm{d}t\, |\phi_i(t)\rangle\, e^{-ik\omega t}, \tag{II.30}$$

$$H(t) = \sum_{k\in\mathbb{Z}} \tilde{H}(k) e^{ik\omega t}, \text{ where } \tilde{H}(k) = \frac{1}{T}\int_0^T \mathrm{d}t\; H(t)\; e^{-ik\omega t}. \tag{II.31}$$

Inserting the expansions into Eq. (II.16), the corresponding Floquet eigenvalue equation in the frequency representation is obtained:

$$\sum_{k'\in\mathbb{Z}} [\tilde{H}(k-k') + \delta_{kk'} k\omega]\, |\tilde{\phi}_i(k')\rangle = \varepsilon_i\, |\tilde{\phi}_i(k)\rangle\,,\ \forall k \in \mathbb{Z}. \tag{II.32}$$

This equation can be written as an infinite-dimensional matrix equation:

$$\underbrace{\begin{pmatrix} \ddots & \ddots & \vdots & \iddots & \iddots \\ \ddots & \tilde{H}(0)+\omega & \tilde{H}(+1) & \tilde{H}(+2) & \iddots \\ \cdots & \tilde{H}(-1) & \tilde{H}(0) & \tilde{H}(+1) & \cdots \\ \iddots & \tilde{H}(-2) & \tilde{H}(-1) & \tilde{H}(0)-\omega & \ddots \\ \iddots & \iddots & \vdots & \ddots & \ddots \end{pmatrix}}_{\tilde{\boldsymbol{H}}_\mathrm{F}} \begin{pmatrix} \vdots \\ |\tilde{\phi}_i(+1)\rangle \\ |\tilde{\phi}_i(0)\rangle \\ |\tilde{\phi}_i(-1)\rangle \\ \vdots \end{pmatrix} = \varepsilon_i \begin{pmatrix} \vdots \\ |\tilde{\phi}_i(+1)\rangle \\ |\tilde{\phi}_i(0)\rangle \\ |\tilde{\phi}_i(-1)\rangle \\ \vdots \end{pmatrix}, \tag{II.33}$$

where all frequency components $|\tilde{\phi}_i(k)\rangle$ have been merged into one vector and similarly for the frequency components of the Hamiltonian.

Formally, this is the frequency domain representation of the abstract Floquet eigenvalue equation (II.23). The i^{th} eigenvector containing all the frequency components corresponds to $||\phi_i\rangle\rangle$ in the abstract formalism. In the same way, the matrix $\tilde{\boldsymbol{H}}_\mathrm{F}$ in Eq. (II.33) is the representation of H_F in the frequency domain. Thus, the significance of Eq. (II.23) is understood: the abstract equation is representation independent, whilst Eq. (II.16) and (II.33) are representations of the same equation in the time and frequency domains, respectively. By noting that $\tilde{H}(-k) = \tilde{H}(k)^\dagger$, it can be seen that $\tilde{\boldsymbol{H}}_\mathrm{F}$ is hermitian. Hence, its eigenvalues, i.e. the quasi-energies ε_i, are real.

With the Hamiltonian $H(t)$ known, the frequency representation of the Floquet states and their corresponding quasi-energies can be found by diagonalising $\tilde{\boldsymbol{H}}_\mathrm{F}$. Since $\tilde{\boldsymbol{H}}_\mathrm{F}$ is infinite-

dimensional, it must first be truncated down to a finite number of dimensions corresponding to frequency components $\{|k| \leq M : k \in \mathbb{Z}\}$ (where appropriate convergence with respect to M is required) [18]. The resulting truncated Hamiltonian can then be diagonalised numerically or using the perturbation theory methods discussed below.

II.2.2 Time-independent degenerate perturbation theory

In this section, a perturbation theory method for finding eigenvectors and eigenvalues of time-independent Hermitian matrices is outlined. This method is based on the one summarised in [6], Appendix A, and can be used to solve equations of the form of Eq. (II.33) perturbatively. This is exactly what is done in the Results chapter of this thesis, for the case of a Hamiltonian with three nearly degenerate eigenvalues. Therefore, the theory will be explicitly outlined for the case of threefold-degenerate eigenvalues. Details of the derivations can be found in [6]; see also [4].

Consider a Hermitian matrix of the form $\boldsymbol{E^0} + \boldsymbol{V}$, where $\boldsymbol{E^0}$ is a diagonal matrix with elements much larger than those of $\boldsymbol{V}$. The eigenvalue equation for $\boldsymbol{E^0} + \boldsymbol{V}$ can be written as

$$(\boldsymbol{E^0} + \boldsymbol{V})\boldsymbol{A} = \boldsymbol{A}\boldsymbol{E}, \tag{II.34}$$

where $\boldsymbol{E}$ is the diagonal matrix of eigenvalues and $\boldsymbol{A}$ is the unitary matrix of eigenvectors, which are sought. Writing out the equation in component form and solving for the components A_{ip}, the relation

$$A_{ip} = \sum_k \frac{V_{ik}A_{kp}}{E_p - E_i^0} \tag{II.35}$$

is obtained [6].

For small perturbations V_{ik}, $E_i^0 \approx E_i$. Thus, for three nearly degenerate eigenvalues of $\boldsymbol{E}^0$, i.e. $E_p^0 \approx E_q^0 \approx E_r^0$, the difference $E_p - E_i^0$ is large with respect to the components V_{ik} for all i except $i \in \{p,q,r\}$. Therefore, A_{ip} is small for all i except $i \in \{p,q,r\}$. The large terms involving A_{pp}, A_{qp} and A_{rp} can then be separated from the rest, resulting in

$$A_{ip} = \frac{V_{ip}A_{pp}}{E_p - E_i^0} + \frac{V_{iq}A_{qp}}{E_p - E_i^0} + \frac{V_{ir}A_{rp}}{E_p - E_i^0} + {\sum_k}' \frac{V_{ik}A_{kp}}{E_p - E_i^0}, \tag{II.36}$$

where the primed sum denotes summation over all $i \notin \{p,q,r\}$. The last term is much smaller than the other three, so the equation can be solved by iteration, when A_{ip}, A_{iq}, A_{ir} are deter-

mined first by the methods described below:

$$\begin{aligned} A_{ip} = &\left[\frac{V_{ip}}{E_p - E_i^0} + \sum_j{}' \frac{V_{ij}V_{jp}}{(E_p - E_i^0)(E_p - E_j^0)} + \dots \right] A_{pp} \\ &+ \left[\frac{V_{iq}}{E_p - E_i^0} + \sum_j{}' \frac{V_{ij}V_{jq}}{(E_p - E_i^0)(E_p - E_j^0)} + \dots \right] A_{qp} \\ &+ \left[\frac{V_{ir}}{E_p - E_i^0} + \sum_j{}' \frac{V_{ij}V_{jr}}{(E_p - E_i^0)(E_p - E_j^0)} + \dots \right] A_{rp}. \end{aligned} \tag{II.37}$$

Setting $i = p,\ i = q$ and $i = r$ in the above equation, three equations for A_{pp}, A_{qp}, and A_{rp} are obtained. These can be written as a single matrix equation:

$$\begin{pmatrix} E_p^0 + \mathcal{V}_{pp}(E_p) & \mathcal{V}_{pq}(E_p) & \mathcal{V}_{pr}(E_p) \\ \mathcal{V}_{qp}(E_p) & E_q^0 + \mathcal{V}_{qq}(E_p) & \mathcal{V}_{qr}(E_p) \\ \mathcal{V}_{rp}(E_p) & \mathcal{V}_{rq}(E_p) & E_r^0 + \mathcal{V}_{rr}(E_p) \end{pmatrix} \begin{pmatrix} A_{pp} \\ A_{qp} \\ A_{rp} \end{pmatrix} = E_p \begin{pmatrix} A_{pp} \\ A_{qp} \\ A_{rp} \end{pmatrix}, \tag{II.38}$$

where

$$\mathcal{V}_{mn}(E) = V_{mn} + \sum_i{}' \frac{V_{mi}V_{in}}{E - E_i^0} + \sum_i{}' \frac{V_{mi}V_{ij}V_{jn}}{(E - E_i^0)(E - E_j^0)} + \dots . \tag{II.39}$$

If the same procedure is applied to the components A_{iq} and A_{ir}, analogous matrix equations are obtained for A_{pq}, A_{qq}, A_{rq} and A_{pr}, A_{qr}, A_{rr}, with E_p replaced by E_q and E_r, respectively. The difference between E_p, E_q and E_r in the $\mathcal{V}$ matrix can be shown to be only a third order effect in the perturbation $\boldsymbol{V}$ [6]. Thus, E_p, E_q and E_r in the matrix on the left-hand side of Eq. (II.38) and the two corresponding matrices for A_{iq} and A_{ir} can be merged into a single variable E, which can be approximated by the mean of the three degenerate eigenvalues E_p^0, E_q^0 and E_r^0. Hence, Eq. (II.38) and the two corresponding equations for A_{iq} and A_{ir} reduce to a single eigenvalue equation for the desired eigenvalues E_p, E_q, E_r and dominant eigenvector components $A_{pp}, A_{qp}, A_{rp},\ A_{pq}, A_{qq}, A_{rq},\ A_{pq}, A_{qq}, A_{rq}$, which can be solved analytically. The other eigenvector components are then given by Eq. (II.37).

II.3 Previous results

The summary of previous results is split into three sections. First, the results found for the simplest version of the model, namely the static network under the Hamiltonian of Eq. (II.1), studied by Walschaers *et al.* [1–3], are presented. Then the initial results for the extension to the vibrating network described by Eq. (II.7), which were recently studied by Brugger [4], are summarised. Finally, some open questions left by the previous work are discussed, which form the basis of the original results of this thesis. Some of the key calculations of previous work

are reproduced in detail, when necessary to understand the original calculations presented in later chapters.

II.3.1 Static network

II.3.1.a Centrosymmetry

The first of the two design principles found for the static network is *centrosymmetry* of the Hamiltonian. To describe centrosymmetry, the exchange operator J is required, which is defined by

$$J_{ij} = \delta_{i,N+1-j}, \tag{II.40}$$

i.e. a matrix with ones on the secondary diagonal and zeros everywhere else. The action of J on a basis vector $|n\rangle \in \mathbb{C}^N$ of the site basis is to flip it to the vector $|N+1-n\rangle$, i.e.

$$J|n\rangle = |N+1-n\rangle, \tag{II.41}$$

in particular $J|\text{in}\rangle = |\text{out}\rangle$ and $J|\text{out}\rangle = |\text{in}\rangle$. Thus J 'reflects' the components of a vector in the site basis about its centre. A Hamiltonian H is said to be centrosymmetric if its commutator with J vanishes:

$$[H, J] = 0. \tag{II.42}$$

If the entries of H are real, as in the cases considered here, then the hermiticity condition of the Hamiltonian reduces to symmetry about the main diagonal. Hence, symmetry plus centrosymmetry implies that the Hamiltonian is symmetric about both diagonals:

$$H_{i,j} = H_{j,i} = H_{N+1-j,N+1-i} = H_{N+1-i,N+1-j}. \tag{II.43}$$

Note that the labelling of the intermediate sites from 2 to $(N-1)$ is ambiguous due to their arrangement in 3D space. Therefore, a Hamiltonian is said to be centrosymmetric if $[H, J] = 0$ for *some* choice of labelling of the intermediate sites. Physically speaking, if a network described by a Hamiltonian is centrosymmetric, then it is appears the same whether viewed from the input or the output site.

Both analytical and numerical methods were used to show that centrosymmetric Hamiltonians are more likely to lead to $\mathscr{P}_{\max} \approx 1$ than completely random realisations [23]. These results can be motivated qualitatively by considering the expansion of $|\psi(t)\rangle$ in the eigenbasis of the Hamiltonian (see Eq. (II.11)):

$$|\psi(t)\rangle = \sum_{i=1}^{N} e^{-iE_i t} \langle \varphi_i | in \rangle |\varphi_i\rangle, \tag{II.44}$$

where $E_i, |\varphi_i\rangle$ are the eigenvalues and eigenvectors of the Hamiltonian. When considering the

transfer probability,

$$\mathscr{P}(t) = \left|\langle \text{out}|\psi(t)\rangle\right|^2 = \left|\sum_{i=1}^{N} e^{-iE_i t}\,\langle \text{out}|\varphi_i\rangle\,\langle\varphi_i|\text{in}\rangle\right|^2, \tag{II.45}$$

it can be seen that in order to obtain $\mathscr{P}(t) \approx 1$ at some time t, the existence of eigenvectors with a high overlap with both $|\text{in}\rangle$ and $|\text{out}\rangle$ is required. With centrosymmetry imposed, high overlap with one of these states automatically guarantees equally high overlap with the other, due to the property of centrosymmetric matrices that for all eigenvectors $|\varphi_i\rangle$,

$$J\,|\varphi_i\rangle = \pm\,|\varphi_i\rangle\,. \tag{II.46}$$

Noting that $J^\dagger J = 1$ and $J^\dagger = J$,

$$\langle \text{out}|\varphi_i\rangle = \langle \text{out}|\,J^\dagger J\,|\varphi_i\rangle = \pm\,\langle \text{in}|\varphi_i\rangle \tag{II.47}$$

$$\Rightarrow \langle \text{out}|\varphi_i\rangle\,\langle\varphi_i|\text{in}\rangle = \pm|\,\langle \text{in}|\varphi_i\rangle\,|^2 = \pm|\,\langle \text{out}|\varphi_i\rangle\,|^2, \tag{II.48}$$

meaning that if there exists an eigenvector with high overlap with $|\text{in}\rangle$, then this eigenvector has the same high overlap with $|\text{out}\rangle$, and vice versa [3, 4]. Therefore, centrosymmetry effectively reduces the number of conditions needed to ensure good transport for a Hamiltonian chosen from a statistical ensemble.

In order to impose centrosymmetry on the Hamiltonian whilst retaining the random matrix characteristics, the distribution of the free matrix elements (i.e. those not fixed by hermiticity or centrosymmetry) must be altered from that of Eq. (II.5) to

$$V_{nm} \sim \begin{cases} \mathscr{N}(0, 2\xi^2) & \text{for } n = m \text{ or } n = N+1-m \\ \mathscr{N}(0, \xi^2) & \text{else} \end{cases}, \tag{II.49}$$

with explicitly fixing $H_{i,j} = H_{j,i} = H_{N+1-j,N+1-i} = H_{N+1-i,N+1-j}$ [3].

II.3.1.b Dominant doublet

The second design principle found for the static case is the so-called *dominant doublet*. To motivate it, consider a system of two sites with Hamiltonian

$$H = \begin{pmatrix} D_1 & V \\ V & D_2 \end{pmatrix}. \tag{II.50}$$

To ensure good transport, let $D_1 = D_2 =: D$, which results in eigenvalues $E_\pm = D \pm V$ and corresponding eigenvectors $|\varphi_\pm\rangle = |\pm\rangle$, with

$$|\pm\rangle := \frac{|\text{in}\rangle \pm |\text{out}\rangle}{\sqrt{2}}. \tag{II.51}$$

The probability of finding the excitation at the output site is

$$\begin{aligned}
\mathscr{P}(t) &= \left|\langle \text{out}|\psi(t)\rangle\right|^2 \\
&= \left|\sum_{i=1}^{N} e^{-iE_i t}\, \langle \text{out}|\varphi_i\rangle\, \langle \varphi_i|\text{in}\rangle\right|^2 \\
&= \left|\sum_{i=1}^{2} e^{-iE_i t}\, \frac{1}{2}\Big[\,|\langle +|\varphi_i\rangle|^2 - |\langle -|\varphi_i\rangle|^2 + \langle +|\varphi_i\rangle\langle \varphi_i|-\rangle - \langle -|\varphi_i\rangle\langle \varphi_i|+\rangle\,\Big]\right|^2 \\
&= \left|\frac{1}{2}e^{-iE_+ t}|\langle +|+\rangle|^2 - \frac{1}{2}e^{-iE_- t}|\langle -|-\rangle|^2\right|^2 \\
&= \frac{1}{2}[1-\cos(2Vt)].
\end{aligned} \tag{II.52}$$

$\mathscr{P}(t)$ oscillates between 0 and 1, thus

$$\mathscr{P}_{\text{max, 2-site}} = 1, \tag{II.53}$$

with the first maximum occurring at

$$\tau_{\text{2-site}} = \frac{\pi}{|E_+ - E_-|} = \frac{\pi}{2|V|}. \tag{II.54}$$

Given that a two-site network with equal on-site energies guarantees perfect transport between the sites, a condition for the eigenvectors of the N-site case is chosen such that favourable properties of the two-site eigenvectors carry over. The Hamiltonian H_0 is required to have two eigenvectors $|\varphi_\pm\rangle$ (with eigenvalues $E_\pm$) that are similar to the $|\pm\rangle$ states:

$$1 \geq |\langle \varphi_\pm|\pm\rangle|^2 > \alpha \approx 1. \tag{II.55}$$

Since the eigenvectors of the Hamiltonian form an orthonormal basis, a relation for the other eigenvectors is obtained:

$$|\langle \varphi_\pm|\mp\rangle|^2 \approx 0,\ |\langle \varphi_i|\pm\rangle|^2 \approx 0,\ \forall\, |\varphi_i\rangle \neq |\varphi_\pm\rangle\,. \tag{II.56}$$

For a rigorous lower bound, the completeness relation for the eigenvectors can be used:

$$\sum_{i=1}^{N} |\varphi_i\rangle\langle \varphi_i| = \mathbb{1}_N \tag{II.57}$$

$$\begin{aligned}
&\Rightarrow 1 = \langle \pm|\pm\rangle = \sum_{i=1}^{N} \langle \pm|\varphi_i\rangle \langle \varphi_i|\pm\rangle = \sum_{i=1}^{N} |\langle \pm|\varphi_i\rangle|^2 \\
&\Rightarrow \sum_{i\neq +}^{N} |\langle +|\varphi_i\rangle|^2 = 1 - |\langle +|\varphi_+\rangle|^2 \leq 1-\alpha, \\
&\quad \sum_{i\neq -}^{N} |\langle -|\varphi_i\rangle|^2 = 1 - |\langle -|\varphi_-\rangle|^2 \leq 1-\alpha.
\end{aligned} \tag{II.58}$$

This means that the $|\varphi_\pm\rangle$ states dominate in the eigenvector expansion of $\left|\langle \text{out}|\psi(t)\rangle\right|^2$ and the calculation becomes reminiscent of the two-site case:

$$\begin{aligned}
\mathscr{P}(t) &= \left|\langle \text{out}|\psi(t)\rangle\right|^2 \\
&= \left| \sum_{i=1}^{N} e^{-iE_i t} \langle \text{out}|\varphi_i\rangle \langle \varphi_i|\text{in}\rangle \right|^2 \\
&= \left| \sum_{i=1}^{N} e^{-iE_i t} \frac{1}{2} \Big[|\langle +|\varphi_i\rangle|^2 - |\langle -|\varphi_i\rangle|^2 + \langle +|\varphi_i\rangle \langle \varphi_i|-\rangle - \langle -|\varphi_i\rangle \langle \varphi_i|+\rangle \Big] \right|^2 \\
&= \frac{1}{4} \left| e^{-iE_+ t} |\langle +|\varphi_+\rangle|^2 - e^{-iE_- t} |\langle -|\varphi_-\rangle|^2 + \sum_{i\neq +}^{N} e^{-iE_i t} |\langle +|\varphi_i\rangle|^2 - \sum_{i\neq -}^{N} e^{-iE_i t} |\langle -|\varphi_i\rangle|^2 \right|^2 .
\end{aligned} \tag{II.59}$$

Note that in the third line, the cross terms $\langle +|\varphi_i\rangle \langle \varphi_i|-\rangle - \langle -|\varphi_i\rangle \langle \varphi_i|+\rangle$ exactly cancel out for all i when centrosymmetry is also imposed:

$$\begin{aligned}
\langle +|\varphi_i\rangle \langle \varphi_i|-\rangle - \langle -|\varphi_i\rangle \langle \varphi_i|+\rangle &= \langle +|\boldsymbol{J}\boldsymbol{J}|\varphi_i\rangle \langle \varphi_i|-\rangle - \langle -|\varphi_i\rangle \langle \varphi_i|\boldsymbol{J}\boldsymbol{J}|+\rangle \\
&= \pm \langle -|\varphi_i\rangle \langle \varphi_i|-\rangle \mp \langle -|\varphi_i\rangle \langle \varphi_i|-\rangle = 0.
\end{aligned} \tag{II.60}$$

Therefore, by considering the upper and lower bounds for the four terms on the right-hand side of Eq. (II.59), for an arbitrarily large reference time T_R, an exact lower bound for $\mathscr{P}_\text{max}$ (using the relation $\alpha^2 \geq 2\alpha - 1$ for $0 < \alpha \leq 1$) is obtained:

$$\mathscr{P}_\text{max} \geq 4\alpha - 3. \tag{II.61}$$

This expression is close to 1 for sufficiently large α. The two small sums contain terms which oscillate at various frequencies, and it was shown that their average contribution can be neglected [3]. Therefore, an accurate approximate bound can be found, which explicitly incorporates T_R:

$$\mathscr{P}_\text{max} \gtrsim \frac{2\alpha - 1}{2} \max_{t\in[0,T_\text{R})} \Big[1 - \cos[(E_+ - E_-)t] \Big]. \tag{II.62}$$

The transfer time occurs at approximately

$$\tau_{N\text{-site}} = \frac{\pi}{|E_+ - E_-|}. \tag{II.63}$$

The condition of Eq. (II.55) is called the *dominant doublet* condition because it enforces two eigenvectors to dominate in the spectral expansion, namely the eigenvectors which resemble the 'doublet' eigenvector structure of the two-site case [3, 4]. Both of these eigenvectors require approximately equal overlap modulus squared with $|\text{in}\rangle$ and $|\text{out}\rangle$, close to 1/2, and therefore centrosymmetry (due to its corollary in Eq. (II.48)) increases the probability of obtaining eigenvectors satisfying the dominant doublet condition.

II.3.1.c Statistics of transfer times

In addition to finding design principles for efficient transport, statistics of transfer times were investigated [3]. Centrosymmetry was imposed on the statistical ensemble of Hamiltonians as per Eq. (II.49) and dominant doublet realisations were post-selected after sampling from the distribution. Then, for realisations satisfying both centrosymmetry and the dominant doublet condition, i.e. the *centrosymmetric dominant doublet ensemble*, the transfer times τ were calculated.

From the definition of $\mathscr{P}_{\max}$ in Eq. (II.4), τ needs to occur within a specified time interval between zero and some reference time T_{R}. For the purpose of the statistical investigation, the reference time was taken to be arbitrarily large so that the full range of transfer times could be investigated. The transfer time of each Hamiltonian was then compared to the corresponding two-site transfer time, i.e. the transfer time that would occur if all the intermediate sites were removed, given by $\tau_{2\text{-site}}$ in Eq. (II.54), with V equal to the input-output site coupling.

The numerical results, supported by analytical calculations, showed a continuous distribution of inverse scaled transfer times $\tau_{2\text{-site}}/\tau$ with a peak between 1.0 and 1.1 and a long tail stretching out to large values of $\tau_{2\text{-site}}/\tau$. This means that there exist realisations of the centrosymmetric dominant doublet ensemble with strongly enhanced (i.e. much faster) transfer times compared to the case of two-sites only (i.e. without the network). As a result, the purpose of the network can be seen: it enables transport to occur between the input and output sites at timescales not possible with only direct coupling between the two sites [3].

II.3.2 Network coupled to vibrations

Moving on to the extended network model with an energy landscape and vibrational coupling as governed by $H(t)$ from Eq. (II.7), the aim is to generalise the design principles found for H_0 to $H(t)$. However, centrosymmetry is broken by the diagonal energy landscape term, H_{D}, so the naïve generalisation to $[H(t), J] = 0$ will not work.

Brugger [4] studied the two-site network of $H(t)$ in detail using Floquet theory and the perturbation theory methods discussed in the previous section. Larger networks were also studied. The formal similarity between the eigenvector expansion under H_0 in Eq. (II.44) (or in general Eq. (II.11)) and the Floquet decomposition under $H(t)$ in Eq. (II.14) is apparent. This

similarity was used to formulate a *dominant Floquet doublet* (DFD) condition analogous to the dominant doublet condition for the static case, albeit valid only for the specific case of $t_0 = 0$, i.e. zero initial phase of the excitation with respect to the external oscillations. For this case it was shown in an analogous manner to Eq. (II.55)–(II.59) that the dominant Floquet doublet condition

$$1 \geq |\langle \phi_{\pm}(0)|\pm\rangle|^2 > \beta \approx 1 \tag{II.64}$$

leads to

$$|\langle \phi_{\pm}(0)|\mp\rangle|^2 \approx 0, |\langle \phi_i(0)|\pm\rangle|^2 \approx 0, \ \forall\, |\phi_i(0)\rangle \neq |\phi_{\pm}(0)\rangle\,, \tag{II.65}$$

and thus

$$\begin{aligned} \mathscr{P}_{\max}(t_0 = 0) &\geq \max_{t\in[0,T_{\mathrm{R}})} \mathscr{P}(t = kT, t_0 = 0) \\ &\gtrsim \frac{2\beta - 1}{2} \max_{t\in[0,T_{\mathrm{R}})} \Big[1 - \cos[(\varepsilon_+ - \varepsilon_-)kT]\Big], \end{aligned} \tag{II.66}$$

where $k \in \mathbb{N}$ and $T = 2\pi/\omega$ is the period of the oscillations in the Hamiltonian. Here, due to the lack of centrosymmetry, the cross terms $\langle +|\phi_i(0)\rangle\langle\phi_i(0)|-\rangle - \langle -|\phi_i(0)\rangle\langle\phi_i(0)|+\rangle$ do not exactly cancel like the analogous cross terms of Eq. (II.60) in the static case. Therefore, an exact bound was not determined. Note that a stroboscopic approach [19] was taken, where the periodicity of the Floquet states was used to consider only $\mathscr{P}(t, t_0 = 0)$ at times $t = kT$, i.e. when the Floquet states $|\phi_i(kT)\rangle = |\phi_i(0)\rangle$, enabling the analogy between the stroboscopic time-evolution and the static one. The transfer time for a dominant Floquet doublet system was found to be approximately

$$\tau_{N\text{-site}} = \frac{\pi}{|\varepsilon_+ - \varepsilon_-|}. \tag{II.67}$$

This relies on the existence of a k such that the sinusoidal oscillation reaches its maximum value in its first period, which was shown hold when the Hamiltonian frequency ω is much larger than $|\varepsilon_+ - \varepsilon_-|$ (see [4], p. 67). The latter assumption was also shown to be valid under the condition that the diagonal on-site energies of H_{static} are much greater than its off-diagonal coupling elements, a condition explicitly incorporated into the model in § II.1. The transfer time for a system with two sites was shown to be

$$\tau_{2\text{-site}} = \frac{\pi}{2|c|}, \tag{II.68}$$

where $2c$ is the value of the off-diagonal elements of H_{vib} in the eigenbasis of H_{static}, which will be explained in § III.2.1.a.

II.3.3 Open questions

The aim of the work started by Brugger [4] was to generalise the design principles found for the static Hamiltonian H_0 to the time-periodic Hamiltonian $H(t)$. An appropriate framework was found in which to study the system under $H(t)$, namely Floquet theory, in which the dominant doublet design principle was successfully generalised, albeit only for the case of when the excitation arrives at the input site at time $t_0 = 0$. This directly leads to three open problems, which form the basis of the results presented in this thesis.

Firstly, a way to generalise the dominant Floquet doublet (DFD) design principle to include any arbitrary initial time t_0 of excitation arrival is required. In general, e.g. in the FMO complex, it is not possible to control at what phase of the external oscillation the energy excitation first comes into the system, i.e. at what time t_0, $|\psi(t_0)\rangle = |\text{in}\rangle$. Therefore, it is essential for the DFD design principle to include, or average over, the effects of t_0.

Secondly, a generalisation of centrosymmetry to some analogous symmetry for the time-periodic case is desired. As stated above, centrosymmetry defined by $[H(t), J] = 0$ is incompatible with the structure of $H(t)$. It may be the case that the appropriate symmetry includes a condition on the the time-dependence of the Hamiltonian. Perhaps this symmetry will let all the cross terms in the eigenvector expansion cancel out, as for centrosymmetry in the static case (Eq. (II.60)). If not, then an upper bound for their contribution needs to be derived, so that an exact bound for $\mathscr{P}_{\max}(t_0)$ can be found.

Finally, once design principles have been found, it is necessary to consider the distribution of transfer times that arise from Hamiltonians satisfying the design principles. Analogous to the discussion in § II.3.1.c, it is desirable to obtain a distribution of transfer times τ where the average τ is not much longer than the corresponding two-site transfer time $\tau_{\text{2-site}}$, and where there exist realisations with strongly enhanced transfer times in comparison to the two-site case. If such desirable statistics of transfer times are found in addition to design principles that produce Hamiltonians with maximum transfer probabilities close to one, then the goal of generalising the model of efficient quantum transport for a static Hamiltonian (presented in [1–3]) to a time-periodic Hamiltonian (initiated in [4]) is achieved.

Chapter III

Results

This chapter presents the original results of this thesis, which provide a solution to the open problems outlined in § II.3.3. First, a generalised symmetry in the Floquet picture is proposed, followed by calculations to determine quantum transport under a simple Hamiltonian exhibiting such a symmetry. Then, a condition on the Floquet states of a Hamiltonian is analytically shown to guarantee efficient transport, supported by numerical simulations. Finally, a statistical investigation into the distribution of transfer times is presented.

III.1 Symmetries of the Hamiltonian

The first aim of this work is to find a generalised symmetry condition for the full Hamiltonian of Eq. (II.7), analogous to centrosymmetry for the static case, which increases the probability of obtaining realisations exhibiting efficient transport. Before any such symmetry condition can be imposed, the symmetries already implicit in the definition of the Hamiltonian must be considered.

III.1.1 Symmetries in space

From Eq. (II.7) above, the Hamiltonian in the site basis is

$$H(t) = \underbrace{\underbrace{\sum_{n=1}^{N} D_n \left|n\right\rangle\left\langle n\right|}_{=:H_\mathrm{D}} + \underbrace{\sum_{n,m}^{N} V_{nm} \left|n\right\rangle\left\langle m\right|}_{=:H_0}}_{=:H_\mathrm{static}} + \cos(\omega t - \delta) \underbrace{\sum_{n,m}^{N} W_{nm} \left|n\right\rangle\left\langle m\right|}_{=:H_\mathrm{vib}}, \tag{II.7}$$

where, on average, D_n is greater than D_{n+1}, resulting in an overall negative 'energy gradient' between the input and output sites. For the static case, the single H_0 term was chosen to be centrosymmetric such that $[H_0, J] = 0$, implying that $V_{n,m} = V_{N+1-n,N+1-m}$. The same condition

cannot be imposed on H_D, since $[H_\mathrm{D}, J] = 0 \Rightarrow D_n = D_{N+1-n}$, which would be inconsistent with the overall energy gradient.

Nevertheless, I found that another simple symmetry with respect to J could be imposed on $H(t)$, which is consistent with the structure of H_D, namely *anti-centrosymmetry*. Analogous to the centrosymmetry condition of Eq. (II.42), a Hamiltonian H is said to be anti-centrosymmetric (or skew-centrosymmetric) [24] if its anti-commutator with J vanishes:

$$\{H, J\} = 0. \tag{III.1}$$

For a real Hamiltonian (and hence symmetric about its main diagonal), this results in the matrix elements satisfying

$$H_{i,j} = H_{j,i} = -H_{N+1-j,N+1-i} = -H_{N+1-i,N+1-j}, \tag{III.2}$$

which is analogous to the centrosymmetry result in Eq. (II.43), but with notable minus signs. Anti-centrosymmetry of a Hamiltonian imposes symmetries on its eigenvector structure, which are expected to lead to good transport properties in the same way as the eigenvector symmetries imposed by centrosymmetry in Eq. (II.48). The mathematical formulation of these symmetries is given below in § III.1.4.

The anti-centrosymmetry condition implies that all matrix elements on the secondary diagonal are zero. This is not desirable for the H_vib term, since the work in [4] showed that transport under a Hamiltonian of the form of $H(t)$ relies on the direct vibrational coupling between the input and output site, i.e. the matrix elements $W_{1N} = W_{N1}$ which lie on the secondary diagonal. Thus, neither of the elementary symmetries considered until now can be imposed on all of the terms in $H(t)$ at once.

III.1.2 Symmetries in time

Nevertheless, it is the *time-periodic* Floquet states of the Hamiltonian which are of interest for transport [4], so the symmetries of the Hamiltonian in time also need to be considered. Moreover, the Floquet states are eigenstates of the Floquet Hamiltonian $H_\mathrm{F} = H(t) - i\partial_t$, so in fact it is the symmetries of this Hamiltonian that need to be considered.

Let us start with simple symmetries analogous to the spatial ones defined with respect to J. To find an analogous operator for functions in $\mathrm{L}^2\big([0,T)\big)$, it is instructive to consider the action of J on a general state vector $|\psi\rangle \in \mathbb{C}^N$, expanded in terms of the site basis vectors $|n\rangle$ as in Eq. (II.24). From Eq. (II.41),

$$J\,|n\rangle = |N+1-n\rangle\,, \tag{II.41}$$

and thus

$$J\,|\psi\rangle = J\sum_{n=1}^{N} c_n\,|n\rangle = \sum_{n=1}^{N} c_n\,|N+1-n\rangle = \sum_{n=1}^{N} c_{N+1-n}\,|n\rangle\,, \tag{III.3}$$

i.e. J 'flips' the components of the state vector. In analogy with the J operator which reflects state vectors $|\psi\rangle \in \mathbb{C}^N$ around their centre, I define the time-reversal operator θ acting on $\mathrm{L}^2\big([0,T)\big)$ by

$$\theta\,|t\rangle = |T-t\rangle \equiv |-t\rangle\,, \tag{III.4}$$

where the $|t\rangle$ are as defined in Eq. (II.25). Here, the periodicity of the $|t\rangle$ states is used to identify $|T-t\rangle$ with $|-t\rangle$. Explicitly, the operation of θ on a general state $|\Psi\rangle \in \mathrm{L}^2\big([0,T)\big)$ can be written as

$$\theta\,|\Psi\rangle = \theta\,\frac{1}{T}\int_0^T \mathrm{d}t\; C(t)|t\rangle = \frac{1}{T}\int_0^T \mathrm{d}t\; C(t)|-t\rangle = \frac{1}{T}\int_0^T \mathrm{d}t\; C(-t)|t\rangle\,. \tag{III.5}$$

Thus, θ simply reverses the sign of the time-argument, just as J exchanges the coefficients c_n and c_{N+1-n}. Note that this time-reversal operator is defined on the space of T-periodic functions, and is not the same as the time-reversal operator that appears in quantum field theory (see e.g. [25]).

With the θ operator in place, the time-dependent parts of H_F, namely $\cos(\omega t-\delta)$ and $i\partial_t$, can be investigated with respect to commutation or anticommutation with θ. Acting on the general function $C(t) \in \mathrm{L}^2\big([0,T)\big)$,

$$\begin{aligned}\theta\;(\cos(\omega t-\delta)\;C(t)) &= \cos(-\omega t-\delta)\;C(-t) = \cos(-\omega t-\delta)\;\theta\;C(t)\\ &= \begin{cases} +\cos(\omega t-\delta)\;\theta\;C(t) & \text{for } \delta\in\{0,\pi\}\\ -\cos(\omega t-\delta)\;\theta\;C(t) & \text{for } \delta\in\{-\frac{\pi}{2},\frac{\pi}{2}\}\end{cases},\end{aligned} \tag{III.6}$$

where in the last equality only the four specific values $-\pi/2, 0, \pi/2, \pi$ of δ are considered. Thus, noting that a cosine phase shifted by $\pi/2$ is a sine, it is apparent that θ commutes with $\cos(\omega t)$, while it anticommutes with $\sin(\omega t)$. For the $i\partial_t$ term, consider the explicit expression for the derivative, with a small parameter $h>0$, and let $t' := t+h > t$. Then,

$$\begin{aligned}\theta\;\big(\partial_t\;C(t)\big) &= \theta\left[\lim_{h\to 0}\frac{C(t+h)-C(t)}{h}\right] = \left[\lim_{h\to 0}\frac{C(-t-h)-C(-t)}{h}\right] = \left[\lim_{h\to 0}\frac{C(-t')-C(-t'+h)}{h}\right]\\ &= -\left[\lim_{h\to 0}\frac{C(-t'+h)-C(-t')}{h}\right] = -\partial_{t'}\;C(-t') = -\partial_t\;C(-t) = -\partial_t\;\big(\theta\;C(t)\big),\end{aligned} \tag{III.7}$$

thus

$$\{i\partial_t,\theta\} = i\{\partial_t,\theta\} = 0. \tag{III.8}$$

III.1.3 Composite symmetries in space and time

With symmetries of both the spatial and temporal components of the Floquet Hamiltonian individually examined, let us consider the effect of the combined symmetry of the two. To this end, I define the *generalised reversal operator*,

$$Þ := J \otimes \theta, \tag{III.9}$$

denoted by the Icelandic letter Þ ('thorn'; for the name *þvervíxlunarvirkinn* which can be constructed in Icelandic to concisely depict the operator). Þ is a tensor product of the exchange operator J on $\mathbb{C}^N$ and the time-reversal operator θ on $\mathrm{L}^2\big([0,T)\big)$ and therefore acts on the space $\mathscr{H}_\mathrm{F} = \mathbb{C}^N \otimes \mathrm{L}^2\big([0,T)\big)$. Since the two constituent spaces are treated independently, when acting on an arbitary state $|\psi(t)\rangle \in \mathscr{H}_\mathrm{F}$, Þ simply reverses both the spatial and the temporal arguments simultaneously:

$$Þ\,|\psi(t)\rangle = J\,|\psi(-t)\rangle\,. \tag{III.10}$$

Explicitly, acting on an abstract Floquet state $||\phi_i\rangle\rangle \in \mathscr{H}_\mathrm{F}$ (given by Eq. (II.26)):

$$Þ\,||\phi_i\rangle\rangle = Þ \sum_{n=1}^{N} \int_0^T \mathrm{d}t\ \phi_i^n(t)\,|n\rangle\otimes|t\rangle = \sum_{n=1}^{N} \int_0^T \mathrm{d}t\ \phi_i^n(t)\,|N{+}1{-}n\rangle\otimes|{-}t\rangle = \sum_{n=1}^{N} \int_0^T \mathrm{d}t\ \phi_i^{N+1-n}(-t)\,|n\rangle\otimes|t\rangle. \tag{III.11}$$

With Þ and H_F both acting on $\mathscr{H}_\mathrm{F}$, commutation and anticommutation relations between the two operators can be investigated. In keeping with the aim of generalising the static condition $[H_0, J] = 0$ to a condition for the time-periodic Hamiltonian, let us see if H_F can be chosen so that it either commutes or anticommutes with Þ. Separating out the spatial and temporal parts of the Hamiltonian,

$$H_\mathrm{F} = (H_\mathrm{D} + H_0) \otimes 1 + H_\mathrm{vib} \otimes \cos(\omega t - \delta) - i\,\mathbb{1}_N \otimes \partial_t \tag{III.12}$$

is obtained, where $\mathbb{1}_N$ is the identity operator on $\mathbb{C}^N$. The last term has already been shown in Eq. (III.8) to anticommute with θ in $\mathrm{L}^2\big([0,T)\big)$ and has a constant function on $\mathbb{C}^N$, so it anticommutes with Þ. Given that one term in H_F always anticommutes with Þ, let us check if all other terms in Þ can be chosen to anticommute with Þ.

From the above discussion, H_D cannot be chosen to commute with J, therefore $H_\mathrm{static} = H_0 + H_\mathrm{D}$ is chosen to anticommute with J so that the first term anticommutes with Þ. Similarly, it has been discussed that H_vib cannot be chosen to anticommute with J (see end of § III.1.1). Hence, for the middle term to anticommute with Þ, H_vib must be chosen to commute with J and $\cos(\omega t - \delta)$ to anticommute with θ. This means that the phase δ must be chosen to be $\pi/2$ such that $\cos(\omega t - \delta) = \sin(\omega t)$. Here it is important to note that the physically relevant quantity is the phase of the oscillation at time t_0 when the excitation first enters the system. Since t_0 can still be arbitrarily chosen in the model, choosing $\delta = \pi/2$ does not result in a loss of generality.

In conclusion, the only commutation or anticommutation relation with respect to simple reversal symmetries in both space and time which can be chosen for the Floquet Hamiltonian H_F is the anticommutation condition

$$\{H_\mathrm{F}, \hat{P}\} = 0. \tag{III.13}$$

To satisfy this condition, the physical Hamiltonian is chosen to be of the form

$$H(t) = \underbrace{H_\mathrm{D} + H_0}_{=H_\mathrm{static}} + \sin(\omega t)\, H_\mathrm{vib}, \tag{III.14}$$

with the individual components chosen under the (anti-)centrosymmetry conditions

$$\{H_\mathrm{static}, J\} = 0, \tag{III.15}$$

$$[H_\mathrm{vib}, J] = 0. \tag{III.16}$$

Let us call the condition of Eq. (III.13) *Floquet antisymmetry*, which will be the proposed generalised symmetry for the time-dependent case.

III.1.4 Eigenvector properties of anticommutating operators

In the static case, centrosymmetry, i.e. the commutation relation $[H_0, J] = 0$, ensured that eigenvectors $|\varphi_i\rangle$ of H_0 all satisfy $J|\varphi_i\rangle = \pm|\varphi_i\rangle$, leading to desirable properties of the eigenvectors (see Eq. (II.48)). For the generalised case of H_F, Floquet antisymmetry, i.e. the anticommutation relation $\{H_\mathrm{F}, \hat{P}\} = 0$, leads to a different, but also desirable, eigenvector property. For every eigenvector $|\phi_i(t)\rangle \in \mathscr{H}_\mathrm{F}$ of H_F with eigenvalue ε_i, $\hat{P}|\phi_i(t)\rangle$ is also an eigenvector of H_F with eigenvalue $-\varepsilon_i$.

This can be easily proven for any two anticommutating operators as follows: Let M and N be two operators on an arbitrary Hilbert space $\mathscr{H}$, such that $\{M, N\} = 0$ and let $|\Phi\rangle \in \mathscr{H}$ be an eigenvector of M with eigenvalue λ. Then

$$MN|\Phi\rangle = -NM|\Phi\rangle = -N\lambda|\Phi\rangle \tag{III.17}$$

$$\Rightarrow M(N|\Phi\rangle) = -\lambda(N|\Phi\rangle). \tag{III.18}$$

Therefore, $N|\Phi\rangle$ is also an eigenvector of M with eigenvalue $-\lambda$ [26].

This property means that all the eigenvectors and eigenvalues of H_F, namely the Floquet states and quasi-energies, come in pairs related by $\hat{P}$; this property will prove to be of great use in the following calculations of transport under a Floquet-antisymmetric Hamiltonian.

III.1.5 Floquet-antisymmetry for enhanced transport

Having identified Floquet-antisymmetry as a potential generalisation of centrosymmetry for the time-dependent case, it remains to be seen whether or not this new symmetry really does enhance the probability of obtaining Hamiltonians that produce efficient transport. To investigate this, I wrote a *Python* program to sample two sets of 1000 Hamiltonians of the form of $H(t)$ as defined in Eq. (II.7), with $N = 8$, one set without any symmetry imposed and one set with the Floquet antisymmetry imposed as defined in Eq. (III.15) and (III.16). The maximum transfer probability $\mathscr{P}_{\max}(t_0)$, as defined by Eq. (II.9), for each Hamiltonian was then calculated using the Floquet methods described in § II.2.1.c and Eq. (II.14), for a uniformly random $t_0 \in [0, T)$. The reference time T_{R} was taken to be $T_{\mathrm{R}} = \tau_{\text{2-site}}$ [3, 4], where $\tau_{\text{2-site}}$ is defined as the transfer time of the corresponding two-site system that would result if the intermediate sites are removed, given by Eq. (II.68). The results of the simulations are shown in Fig. III.1.

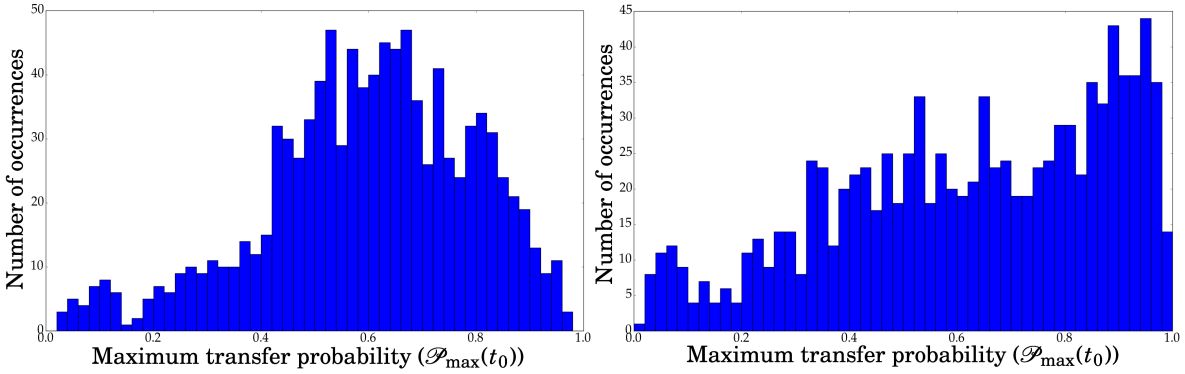

Figure III.1: Histograms showing the distribution of $\mathscr{P}_{\max}(t_0)$ for 1000 time-periodic Hamiltonians of the form of Eq. (II.7) from two different ensembles. The graphs were generated in *Python* using numerical Floquet methods as described in § II.2.1.c. (a) depicts the results from a random GOE ensemble with the individual terms of the Hamiltonian taken of the forms defined in § II.1 with parameters $\xi = \eta = 1$, $D_0 = 10$, $\sigma = 0.02$, $N = 8$ (arbitrary units). The initial phase $t_0 \in [0, T)$ was sampled from a uniform distribution in $[0, T)$. The reference time $T_{\mathrm{R}} = \tau_{\text{2-site}}$ was explicitly calculated for the corresponding system with the six intermediate sites removed. (b) depicts the results from a random GOE ensemble with Floquet-antisymmetry imposed as defined in Eq. (III.15) and (III.16). The statistical parameters for the remaining independent variables are the same as in (a). Note that the vertical axis on the two plots have been scaled independently to their respective maximum values.

The figure shows a stark difference between the probability of obtaining Hamiltonians with $\mathscr{P}_{\max}(t_0) > 0.9$ for the two sets of Hamiltonians, 16% for the Floquet-antisymmetric ones compared to 5% for the others. The Floquet antisymmetry is indeed found to significantly increase the probability of obtaining $\mathscr{P}_{\max}(t_0) > 0.9$ for a randomly sampled Hamiltonian and can therefore, at least statistically, be considered a design principle for efficient transport. Explaining

why Floquet antisymmetry leads to efficient transport is the subject of the following sections.

III.2 Transport under a Floquet-antisymmetric Hamiltonian

In order to understand how Floquet antisymmetry may enhance transport efficiency, let us analytically calculate the Floquet states and quasi-energies of a Floquet-antisymmetric Hamiltonian, which is practical for 2×2 or 3×3 Hamiltonians. Detailed calculations using perturbation theory for the 2×2 case, without any specific symmetry imposed, were performed in [4]. Given that only two sites are present, perfect transport was shown to always occur under specific conditions. The three-site case is the simplest case in which an intermediate site between the input and output sites is present, such that the idea of a *network* makes sense. It is also the simplest case in which anti-centrosymmetry can be meaningfully imposed on the matrices, since a 2×2 anti-centrosymmetric Hamiltonian is diagonal. Therefore, in the following let us compute the Floquet states and quasi-energies for a 3×3 Hamiltonian of the form of Eq. (III.14), and then investigate the resulting transport. The method used to compute the Floquet states roughly follows that in [4] and [6].

III.2.1 Calculation for a three-site Hamiltonian

The most general form of a 3×3 Floquet-antisymmetric Hamiltonian of the form in Eq. (III.14), in the site basis, is

$$H(t)=\underbrace{\begin{pmatrix} D & V & 0\\ V & 0 & -V\\ 0 & -V & -D\end{pmatrix}}_{=H_{\text{static}}}+\sin(\omega t)\underbrace{\begin{pmatrix} W_{11} & W_{12} & W_{13}\\ W_{12} & W_{22} & W_{12}\\ W_{13} & W_{12} & W_{11}\end{pmatrix}}_{=H_{\text{vib}}}. \tag{III.19}$$

Before the perturbation methods presented in § II.2.2 can be applied to this Hamiltonian, a number of transformations need to be carried out.

III.2.1.a Basis transformation

First, the time-independent term H_{static} in the site basis $\mathscr{B}$ is diagonalised, such that the whole Hamiltonian is expressed in the eigenbasis of H_{static}, the so-called *energy basis*, $\mathscr{E}$. Explicit calculation reveals that the eigenvalues E_i and eigenvectors $|\varphi_i\rangle$ of H_{static} are complicated functions of the matrix elements D and V. However, remembering the initial formulation of the model in § II.1, the diagonal elements $\pm D$ (representing on-site energies) will be an order of magnitude larger than the off-diagonal elements $\pm V$ (representing static couplings). Therefore,

V/D can be considered as a small parameter, denoted by v, with

$$v^2 \ll 1. \tag{III.20}$$

This allows the eigenvectors and eigenvalues to be expanded in this small parameter, which up to second order in v gives

$$E_1 = D\left(1+v^2\right),\ \ E_2 = 0,\ \ E_3 = -D\left(1+v^2\right), \tag{III.21}$$

and

$$|\varphi_1\rangle = \begin{pmatrix} 1-\frac{1}{2}v^2 \\ v \\ -\frac{1}{2}v^2 \end{pmatrix}_{\mathscr{B}},\ \ |\varphi_2\rangle = \begin{pmatrix} -v \\ 1-v^2 \\ -v \end{pmatrix}_{\mathscr{B}},\ \ |\varphi_3\rangle = \begin{pmatrix} -\frac{1}{2}v^2 \\ v \\ 1-\frac{1}{2}v^2 \end{pmatrix}_{\mathscr{B}}. \tag{III.22}$$

The property of anti-centrosymmetric matrices (§ III.1.4), where the eigenvectors come in pairs of $|\varphi_i\rangle$ and $J|\varphi_i\rangle$ and eigenvalues come in pairs of E_i and $-E_i$, can be seen explicitly, namely

$$\begin{aligned} E_1 = -E_3,\ \ E_2 = -E_2, \\ J|\varphi_1\rangle = |\varphi_3\rangle,\ \ J|\varphi_2\rangle = |\varphi_2\rangle. \end{aligned} \tag{III.23}$$

The $|\varphi_i\rangle$ are the basis vectors of the energy basis $\mathscr{E}$, expressed above in the site basis $\mathscr{B}$. For small v, it can be seen that the $|\varphi_i\rangle$ are similar to the basis vectors of the site basis $|n\rangle$, with $|1\rangle = (1,0,0)_{\mathscr{B}}$ etc. In the same way, the energy eigenvalues E_i are close to the on-site energies $-D, 0, D$.

The transformed Hamiltonian in the energy basis is given by

$$H_{\mathscr{E}}(t) = UH_{\mathscr{B}}(t)U^\dagger = \underbrace{UH_{\text{static},\mathscr{B}}U^\dagger}_{=:H_{\text{static},\mathscr{E}}} + \sin(\omega t)\ \underbrace{UH_{\text{vib},\mathscr{B}}U^\dagger}_{=:H_{\text{vib},\mathscr{E}}}, \tag{III.24}$$

where U is the unitary matrix of eigenvectors of H_{static}:

$$U = \begin{pmatrix} 1-\frac{1}{2}v^2 & v & -\frac{1}{2}v^2 \\ v & -1+v^2 & v \\ -\frac{1}{2}v^2 & v & 1-\frac{1}{2}v^2 \end{pmatrix}_{\mathscr{B}} \tag{III.25}$$

Given that the anti-centrosymmetry of $H_{\text{static},\mathscr{B}}$ ensures that its eigenvectors come in pairs of $|\varphi_i\rangle$ and $J|\varphi_i\rangle$, the matrix $U = U^\dagger$ is centrosymmetric, i.e. $[U, J] = 0$. As a result,

$$\{H_{\text{static},\mathscr{E}}, J\} = \{UH_{\text{static},\mathscr{B}}U^\dagger, J\} = U\{H_{\text{static},\mathscr{B}}, J\}U^\dagger = 0, \tag{III.26}$$

$$[H_{\text{vib},\mathscr{E}}, J] = [UH_{\text{vib},\mathscr{B}}U^\dagger, J] = U[H_{\text{vib},\mathscr{B}}, J]U^\dagger = 0, \tag{III.27}$$

so the basis transformation preserves the anti-centrosymmetry and centrosymmetry, respectively, of its constituent terms. Therefore, the composite Floquet antisymmetry is also preserved, namely $\{H_{\mathrm{F},\mathscr{E}}, \bar{P}\} = 0$.

In matrix form, the most general form of the Hamiltonian in the energy basis, with Floquet-antisymmetry imposed, is then

$$H(t) = \underbrace{\begin{pmatrix} E & 0 & 0 \\ 0 & 0 & 0 \\ 0 & 0 & -E \end{pmatrix}_{\mathscr{E}}}_{=H_{\mathrm{static},\mathscr{E}}} + 2\sin(\omega t) \underbrace{\begin{pmatrix} a & b & c \\ b & d & b \\ c & b & a \end{pmatrix}_{\mathscr{E}}}_{=H_{\mathrm{vib},\mathscr{E}}}, \tag{III.28}$$

where $E \coloneqq E_1$ and $a, b, c, d \in \mathbb{R}$, with the factor of two added to simplify the following calculations. Given that the site and energy bases are not too different from one another, the individual matrix elements of $H_{\mathrm{vib},\mathscr{E}}$, namely a, b, c, d, will be of the same order of magnitude as the matrix elements of $H_{\mathrm{vib},\mathscr{B}}$, i.e. W_{nm}.

III.2.1.b Phase transformation

In order to simplify calculations, a phase transformation to the rotating frame associated with the oscillation frequency ω is performed. In the energy basis, any state $|\psi(t)\rangle \in \mathbb{C}^3$ can be expanded as

$$|\psi(t)\rangle = c_1(t)|\varphi_1\rangle + c_2(t)|\varphi_2\rangle + c_3(t)|\varphi_3\rangle = \begin{pmatrix} c_1(t) \\ c_2(t) \\ c_3(t) \end{pmatrix}_{\mathscr{E}}, \tag{III.29}$$

with time-dependent amplitudes $c_1(t), c_2(t), c_3(t)$, and evolves under the Schrödinger equation

$$H(t)|\psi(t)\rangle = i\partial_t |\psi(t)\rangle . \tag{III.30}$$

Now, a new set of phase-transformed amplitudes is introduced, namely

$$\begin{aligned} c_1'(t) &= e^{i\frac{\omega}{2}t} c_1(t), \\ c_2'(t) &= e^{i0t}\ c_2(t), \\ c_3'(t) &= e^{-i\frac{\omega}{2}t} c_3(t), \end{aligned} \tag{III.31}$$

where a prime is used to denote phase transformed quantities. Substituting into the Schrödinger equation, the problem can be re-expressed in terms of a phase-transformed state

$$|\psi'(t)\rangle = c_1'(t)|\varphi_1\rangle + c_2'(t)|\varphi_2\rangle + c_3'(t)|\varphi_3\rangle = \begin{pmatrix} c_1'(t) \\ c_2'(t) \\ c_3'(t) \end{pmatrix}_{\mathscr{E}}, \tag{III.32}$$

evolving under the Schrödinger equation

$$H'(t)\,|\psi'(t)\rangle = i\partial_t\,|\psi'(t)\rangle\,, \tag{III.33}$$

with the phase-transformed Hamiltonian found to be

$$H'(t) = \begin{pmatrix} \Delta - ia\left(e^{i\omega t} - e^{-i\omega t}\right) & -ib\left(e^{i\frac{3\omega}{2}t} - e^{-i\frac{\omega}{2}t}\right) & -ic\left(e^{i2\omega t} - 1\right) \\ ib\left(e^{-i\frac{3\omega}{2}t} - e^{i\frac{\omega}{2}t}\right) & -id\left(e^{i\omega t} - e^{-i\omega t}\right) & -ib\left(e^{i\frac{3\omega}{2}t} - e^{-i\frac{\omega}{2}t}\right) \\ ic\left(e^{-i2\omega t} - 1\right) & ib\left(e^{-i\frac{3\omega}{2}t} - e^{i\frac{\omega}{2}t}\right) & -\Delta - ia\left(e^{i\omega t} - e^{-i\omega t}\right) \end{pmatrix}_{\mathscr{E}}. \tag{III.34}$$

Here, considering the case of near-resonant driving, a small parameter Δ has been defined by

$$\Delta \coloneqq \frac{\omega_0 - \omega}{2}, \tag{III.35}$$

where ω_0 is defined as the difference between the energy eigenvalues $E_1 - E_N$, in this case $\omega_0 \coloneqq 2E$. Exact resonance occurs for $\Delta = 0$, i.e. when the driving frequency exactly equals the difference between the energy eigenvalues [4]. $H'(t)$ is time-periodic, with period $\omega/2$, enabling the use of Floquet theory.

III.2.1.c Fourier transformation

Using Eq. (II.31), $[H'(t) - i\partial_t]$ can be Fourier transformed into an infinite dimensional matrix $\tilde{\boldsymbol{H}}'_{\mathrm{F}}$ of the form of Eq. (II.33), with blocks $\tilde{H}'(k)$. Each $\tilde{H}'(k)$ is obtained by integrating $H'(t)\,e^{-ik\omega t/2}$ over one time period $2T$, thus picking out the terms from $H'(t)$ that oscillate at exactly the frequency $k\omega/2$. The Fourier transformed Hamiltonian truncated down to 5×5 blocks (the minimum needed to see each non-vanishing block at least once) is shown in Fig. III.2. The blocks corresponding to $\tilde{H}'(0) + k\frac{\omega}{2}\mathbb{1}_3$ are highlighted for emphasis.

III.2.1.d Perturbation theory calculations

The Fourier transformed Hamiltonian $\tilde{\boldsymbol{H}}'_{\mathrm{F}}$ contains matrix elements of two distinct orders of magnitude: large terms proportional to $\omega \approx 2E$ and small terms proportional to the elements a, b, c, d of $H_{\mathrm{vib},\mathscr{E}}$, with the addition of another set of small terms due to the de-tuning parameter Δ. This allows the perturbation theory methods described in § II.2.2 to be used on $\tilde{\boldsymbol{H}}'_{\mathrm{F}}$. The matrix is split up as $\tilde{\boldsymbol{H}}'_{\mathrm{F}} = (\boldsymbol{E^0} + \boldsymbol{V})$, corresponding to Eq. (II.34), with $\boldsymbol{E^0}$ involving only factors of ω on the diagonal, while $\boldsymbol{V}$ contains all the other (smaller) terms.

The elements of the central block of $\tilde{\boldsymbol{H}}'_{\mathrm{F}}$ are assigned row and column indices (p, q, r) corresponding to the notation in § II.2.2. Then, the diagonal elements of the central block of $\boldsymbol{E^0}$, all zeros, are taken as the three degenerate eigenvalues of $\boldsymbol{E^0}$ with the corresponding eigenvalues of $(\boldsymbol{E^0} + \boldsymbol{V})$ being the desired quasi-energies $\varepsilon'_i,\ i \in \{1,2,3\}$. From Eq. (II.33), the corresponding eigenvectors are the central ($k = 0$) Fourier components $|\tilde{\phi}_i{}'(k=0)\rangle\,,\ i \in \{1,2,3\}$, with the other

$$\tilde{\boldsymbol{H}}'_{\mathrm{F}} = \left(\begin{array}{c|ccc|ccc|ccc|ccc|ccc|c}
\ddots & \multicolumn{3}{c|}{\vdots} & \multicolumn{3}{c|}{\vdots} & \multicolumn{3}{c|}{\vdots} & \multicolumn{3}{c|}{\vdots} & \multicolumn{3}{c|}{\vdots} & \iddots \\
\hline
 & \omega+\Delta & 0 & ic & 0 & 0 & 0 & -ia & 0 & 0 & 0 & -ib & 0 & 0 & 0 & -ic & \\
\cdots & 0 & \omega & 0 & -ib & 0 & 0 & 0 & -id & 0 & 0 & 0 & -ib & 0 & 0 & 0 & \cdots \\
 & -ic & 0 & \omega-\Delta & 0 & -ib & 0 & 0 & 0 & -ia & 0 & 0 & 0 & 0 & 0 & 0 & \\
\hline
 & 0 & ib & 0 & \frac{\omega}{2}+\Delta & 0 & ic & 0 & 0 & 0 & -ia & 0 & 0 & 0 & -ib & 0 & \\
\cdots & 0 & 0 & ib & 0 & \frac{\omega}{2} & 0 & -ib & 0 & 0 & 0 & -id & 0 & 0 & 0 & -ib & \cdots \\
 & 0 & 0 & 0 & -ic & 0 & \frac{\omega}{2}-\Delta & 0 & -ib & 0 & 0 & 0 & -ia & 0 & 0 & 0 & \\
\hline
 & ia & 0 & 0 & 0 & ib & 0 & \Delta & 0 & ic & 0 & 0 & 0 & -ia & 0 & 0 & \\
\cdots & 0 & id & 0 & 0 & 0 & ib & 0 & 0 & 0 & -ib & 0 & 0 & 0 & -id & 0 & \cdots \\
 & 0 & 0 & ia & 0 & 0 & 0 & -ic & 0 & -\Delta & 0 & -ib & 0 & 0 & 0 & -ia & \\
\hline
 & 0 & 0 & 0 & ia & 0 & 0 & 0 & ib & 0 & -\frac{\omega}{2}+\Delta & 0 & ic & 0 & 0 & 0 & \\
\cdots & ib & 0 & 0 & 0 & id & 0 & 0 & 0 & ib & 0 & -\frac{\omega}{2} & 0 & -ib & 0 & 0 & \cdots \\
 & 0 & ib & 0 & 0 & 0 & ia & 0 & 0 & 0 & -ic & 0 & -\frac{\omega}{2}-\Delta & 0 & -ib & 0 & \\
\hline
 & 0 & 0 & 0 & 0 & 0 & 0 & ia & 0 & 0 & 0 & ib & 0 & -\omega+\Delta & 0 & ic & \\
\cdots & 0 & 0 & 0 & ib & 0 & 0 & 0 & id & 0 & 0 & 0 & ib & 0 & -\omega & 0 & \cdots \\
 & ic & 0 & 0 & 0 & ib & 0 & 0 & 0 & ia & 0 & 0 & 0 & -ic & 0 & -\omega-\Delta & \\
\hline
\iddots & \multicolumn{3}{c|}{\vdots} & \multicolumn{3}{c|}{\vdots} & \multicolumn{3}{c|}{\vdots} & \multicolumn{3}{c|}{\vdots} & \multicolumn{3}{c|}{\vdots} & \ddots
\end{array}\right). \tag{III.36}$$

Figure III.2: The Fourier transformed Hamiltonian $\tilde{\boldsymbol{H}}'_{\mathrm{F}}$, truncated to 5×5 blocks.

Fourier components given by Eq. (II.37). The perturbation theory is performed to first order in both of the small parameters that appear in the calculations:

$$\frac{H_{\mathrm{vib},\mathscr{E},mn}}{\omega} \text{ and } \frac{\Delta}{\omega}, \tag{III.37}$$

where the matrix elements $H_{\mathrm{vib},\mathscr{E},mn}$ are given by a,b,c,d.

Explicit calculations using Eq. (II.39), omitted here for brevity, reveal that the first-order effective eigenvalue equation, Eq. (II.38), for $\tilde{\boldsymbol{H}}'_{\mathrm{F}}$ is

$$\begin{pmatrix} \Delta-\frac{4}{3}\frac{b^2}{\omega}+\frac{c^2}{2\omega} & 0 & -ic \\ 0 & 0 & 0 \\ ic & 0 & -\Delta+\frac{4}{3}\frac{b^2}{\omega}-\frac{c^2}{2\omega} \end{pmatrix}\begin{pmatrix} A_{pp} \\ A_{qp} \\ A_{rp} \end{pmatrix} = E_p \begin{pmatrix} A_{pp} \\ A_{qp} \\ A_{rp} \end{pmatrix}. \tag{III.38}$$

The zeros in the matrix on the left-hand side are due to the anti-centrosymmetry of H_{vib} and effectively reduce this 3×3 eigenvalue equation to a 2×2 one. The equation can be solved

analytically, which when keeping only terms to first order results in the eigenvalues

$$\begin{aligned}
\varepsilon_1' &= E_p = \sqrt{c^2+\Delta^2+\frac{\Delta}{\omega}\left(c^2-\frac{8}{3}b^2\right)},\\
\varepsilon_2' &= E_q = 0,\\
\varepsilon_3' &= E_r = -\sqrt{c^2+\Delta^2+\frac{\Delta}{\omega}\left(c^2-\frac{8}{3}b^2\right)} = -\varepsilon_1',
\end{aligned} \tag{III.39}$$

and corresponding eigenvectors

$$\begin{aligned}
|\tilde{\phi}_1'(k=0)\rangle &= \frac{1}{\sqrt{2A}}\begin{pmatrix} B\left[1-\frac{1}{2}\left(l-\frac{h}{A}\right)\right]+\frac{lA-h}{B} \\ 0 \\ \frac{i}{B}\left[1-\frac{1}{2}\left(l-\frac{h}{A}\right)\right] \end{pmatrix}_{\mathscr{E}},\\
|\tilde{\phi}_2'(k=0)\rangle &= \begin{pmatrix} 0 \\ 1 \\ 0 \end{pmatrix}_{\mathscr{E}},\\
|\tilde{\phi}_3'(k=0)\rangle &= \frac{1}{\sqrt{2A}}\begin{pmatrix} \frac{i}{B}\left[1-\frac{1}{2}\left(l-\frac{h}{A}\right)\right] \\ 0 \\ B\left[1-\frac{1}{2}\left(l-\frac{h}{A}\right)\right]+\frac{lA-h}{B} \end{pmatrix}_{\mathscr{E}} = \hat{P}\,|\tilde{\phi}_1'(k=0)\rangle\,,
\end{aligned} \tag{III.40}$$

where the variables A and B of zero-th order and the first-order parameters l and h have been introduced to simplify the notation, with

$$\begin{aligned}
A &:= \sqrt{1+\left(\frac{\Delta}{c}\right)^2},\quad B := \sqrt{\sqrt{1+\left(\frac{\Delta}{c}\right)^2}+\frac{\Delta}{c}},\\
l &:= \frac{1}{2A}\frac{\Delta}{\omega}\left(1-\frac{16}{6}\frac{b^2}{c^2}\right),\quad h := \frac{8b^2-3c^2}{6c\omega}.
\end{aligned} \tag{III.41}$$

Note that at exact resonance, i.e. for $\Delta = 0$, $A = B = 1$ and $l = 0$.

Calculating the $k = \pm 1$ Fourier components using Eq. (II.37), the Floquet states in the time domain can finally be determined using the Fourier expansion of Eq. (II.30), assuming that the $k = 0, \pm 1$ components dominate in the expansion. Keeping again only terms up to first order, the Floquet states (normalised up to second order terms) are

$$|\phi_1'(t)\rangle = \frac{1}{\sqrt{2A}}\begin{pmatrix} B\left[1-\frac{1}{2}\left(l-\frac{h}{A}\right)\right]+\frac{lA-h}{B} \\ 2\frac{b}{\omega}\left[-iB\,e^{i\frac{\omega}{2}t}+\frac{1}{B}e^{-i\frac{\omega}{2}t}\right] \\ \frac{i}{B}\left[1-\frac{1}{2}\left(l-\frac{h}{A}\right)\right] \end{pmatrix}_{\mathscr{E}},$$

$$|\phi_2'(t)\rangle = \begin{pmatrix} -2i\frac{b}{\omega}e^{-i\frac{\omega}{2}t} \\ 1 \\ -2i\frac{b}{\omega}e^{i\frac{\omega}{2}t} \end{pmatrix}_{\mathscr{E}}, \tag{III.42}$$

$$|\phi_3'(t)\rangle = \frac{1}{\sqrt{2A}} \begin{pmatrix} \frac{i}{B}\left[1-\frac{1}{2}\left(l-\frac{h}{A}\right)\right] \\ 2\frac{b}{\omega}\left[-iB\ e^{-i\frac{\omega}{2}t}+\frac{1}{B}e^{i\frac{\omega}{2}t}\right] \\ B\left[1-\frac{1}{2}\left(l-\frac{h}{A}\right)\right]+\frac{lA-h}{B} \end{pmatrix}_{\mathscr{E}} = \Pr|\phi_1'(t)\rangle,$$

where by comparing with Eq. (III.40), it can be seen that all terms coming from the $k = \pm 1$ components come with factors of the first-order term b/ω.

III.2.1.e Inverse phase transformation

The inverse phase transformation to the one applied to the Hamiltonian can now be applied to the Floquet states. Considering the form of the phase transformation from Eq. (III.31), this simply amounts to multiplying the first and last elements of each vector by $e^{-i\frac{\omega}{2}t}$ and $e^{i\frac{\omega}{2}t}$, respectively. The states resulting from an inverse phase transformation of the Floquet states of H_{F}' together with the unaltered quasi-energies ε_1' are a valid choice of Floquet states and quasi-energies of H_{F}, as can be verified by substituting into Eq. (II.14).

Thus, the Floquet states in the original frame (in the energy basis) are

$$|\phi_1(t)\rangle = \frac{1}{\sqrt{2A}} \begin{pmatrix} \left\{B\left[1-\frac{1}{2}\left(l-\frac{h}{A}\right)\right]+\frac{lA-h}{B}\right\} e^{-i\frac{\omega}{2}t} \\ 2\frac{b}{\omega}\left[-iB\ e^{i\frac{\omega}{2}t}+\frac{1}{B}e^{-i\frac{\omega}{2}t}\right] \\ \frac{i}{B}\left[1-\frac{1}{2}\left(l-\frac{h}{A}\right)\right] e^{i\frac{\omega}{2}t} \end{pmatrix}_{\mathscr{E}},$$

$$|\phi_2(t)\rangle = \begin{pmatrix} -2i\frac{b}{\omega}e^{-i\omega t} \\ 1 \\ -2i\frac{b}{\omega}e^{i\omega t} \end{pmatrix}_{\mathscr{E}}, \tag{III.43}$$

$$|\phi_3(t)\rangle = \frac{1}{\sqrt{2A}} \begin{pmatrix} \frac{i}{B}\left[1-\frac{1}{2}\left(l-\frac{h}{A}\right)\right] e^{-i\frac{\omega}{2}t} \\ 2\frac{b}{\omega}\left[-iB\ e^{-i\frac{\omega}{2}t}+\frac{1}{B}e^{i\frac{\omega}{2}t}\right] \\ \left\{B\left[1-\frac{1}{2}\left(l-\frac{h}{A}\right)\right]+\frac{lA-h}{B}\right\} e^{i\frac{\omega}{2}t} \end{pmatrix}_{\mathscr{E}},$$

with the corresponding quasi-energies unchanged from the transformation, i.e.

$$\varepsilon_1 = \sqrt{c^2+\Delta^2+\frac{\Delta}{\omega}\left(c^2-\frac{8}{3}b^2\right)},\ \ \varepsilon_2 = 0,\ \ \varepsilon_3 = -\sqrt{c^2+\Delta^2+\frac{\Delta}{\omega}\left(c^2-\frac{8}{3}b^2\right)}. \tag{III.44}$$

The symmetries resulting from the Floquet antisymmetry of H_{F}, i.e. that $\{H_{\mathrm{F}},\Pr\} = 0$, are ap-

parent:

$$\begin{gathered}\varepsilon_1 = -\varepsilon_3,\ \ \varepsilon_2 = -\varepsilon_2, \\ \hat{P}\,|\phi_1(t)\rangle = |\phi_3(t)\rangle\,,\ \ \hat{P}\,|\phi_2(t)\rangle = |\phi_2(t)\rangle\,,\end{gathered} \tag{III.45}$$

as expected.

III.2.1.f Transport in the energy basis

Under the assumption that $v^2 = (V/D)^2 \ll 1$, i.e. that the diagonal elements of H_{static} are much greater than its off-diagonal elements, the basis vectors of the energy basis $|\varphi_i\rangle$ (eigenvectors of H_{static}) are similar to the basis vectors of the site basis $|n\rangle$ (see discussion in § III.2.1.a). In general, the Floquet states in the site basis will be of a much more complicated form than the ones in the energy basis above. Therefore, before finally calculating the Floquet states in the site basis, it is informative to calculate 'transport' in the energy basis between the energy eigenstates corresponding to the highest and lowest energy eigenvalues, $|\varphi_1\rangle$ and $|\varphi_3\rangle$. This would be equivalent to transport between $|\text{in}\rangle$ and $|\text{out}\rangle$ in the limit of $v \to 0$.

Expanding the state of the system $|\psi(t)\rangle$ in terms of the Floquet states in the energy basis $|\phi_i(t)\rangle$, using Eq. (II.14), the probability of finding the system at time t in the energy eigenstate $|\varphi_3\rangle$, with the initial condition $|\psi(t=t_0)\rangle = |\varphi_1\rangle$, is

$$\begin{aligned}\left|\langle\varphi_3|\psi(t,t_0)\rangle\right|^2 &= \left|\sum_{i=1}^{3} e^{-i\varepsilon_i(t-t_0)}\,\langle\varphi_3|\phi_i(t)\rangle\,\langle\phi_i(t_0)|\varphi_1\rangle\right|^2 \\ &= \left|e^{-i\varepsilon_1(t-t_0)}\,\langle\varphi_3|\phi_1(t)\rangle\,\langle\phi_1(t_0)|\varphi_1\rangle + 0 + e^{-i(-\varepsilon_1)(t-t_0)}\,\langle\varphi_3|\phi_3(t)\rangle\,\langle\phi_3(t_0)|\varphi_1\rangle\right|^2 \\ &= \left|\frac{i}{2A}e^{-i\varepsilon_1(t-t_0)}e^{i\frac{\omega}{2}(t+t_0)}\left[1-\frac{l-\frac{h}{A}}{1+\frac{c}{\Delta}A}\right] - \frac{i}{2A}e^{i\varepsilon_1(t-t_0)}e^{i\frac{\omega}{2}(t+t_0)}\left[1-\frac{l-\frac{h}{A}}{1+\frac{c}{\Delta}A}\right]\right|^2 \\ &= \frac{1}{A^2}\left[1-\frac{l-\frac{h}{A}}{1+\frac{c}{\Delta}A}\right]^2 \frac{\left[1-\cos\left[2\varepsilon_1(t-t_0)\right]\right]}{2},\end{aligned} \tag{III.46}$$

where, as defined by Eq. (III.41), A is a zero-th order parameter and l, h are perturbation parameters of first order. To first order in h and l, the maximum of this sinusoidal transfer probability is

$$\frac{1}{A^2}\left[1-2\frac{l-\frac{h}{A}}{1+\frac{c}{\Delta}A}\right], \tag{III.47}$$

which is close to 1 for small perturbation parameters h, l, as desired. In the limit of $\Delta \to 0$, i.e. for the driving frequency ω approaching the difference between the energy eigenvalues

$\omega_0 = E_1 - E_3 = 2E$, $A = 1$, $l = 0$ and $(c/\Delta) \to \infty$, so that

$$\left|\langle\varphi_3|\psi(t,t_0)\rangle\right|^2 \to \frac{1}{2}\Big(1 - \cos\left[2c(t-t_0)\right]\Big), \tag{III.48}$$

i.e. the probability oscillates sinusoidally with a maximum of exactly 1, with frequency equal to the vibrational coupling $2c$ between the top and bottom energy eigenstates. In this case, no first order terms in $H_{\text{vib},\mathscr{E},mn}/\omega$ survive the modulus squared. Since, as previously stated, all terms from Fourier components $|k| > 0$ come with factors of first order terms, this means that in the limit $\Delta \to 0$, the $k = 0$ Fourier component is the only Fourier component contributing to transport in the energy basis.

Taking a step back, the effect of the Floquet antisymmetry imposed at the beginning can now be understood. The perfect matching of the two terms corresponding to the first and third energy eigenstates in line three of Eq. (III.46), in both amplitude and phase, is due to the symmetries stated in Eq. (III.45). These symmetries follow from Floquet antisymmetry and make the transport probability oscillate sinusoidally with amplitude of 1.

III.2.1.g Transport in the site basis

With close-to-perfect transport established in the energy basis, let us finally return to the site basis to investigate the physical energy transport from site $|\text{in}\rangle$ to site $|\text{out}\rangle$. Considering the expression for the eigenvectors of the energy basis $|\varphi_i\rangle$ in Eq. (III.22), the $|\varphi_i\rangle$ can be seen as simply the basis vectors $|n\rangle$ of the site basis plus a small perturbation v. The 'resonant' Floquet states expressed in the site basis are given by

$$|\phi_i(t)\rangle_{\mathscr{B}} = U^\dagger |\phi_i(t)\rangle_{\mathscr{E}}\,, \tag{III.49}$$

where U is the unitary matrix of the energy basis eigenvectors, given by Eq. (III.25).

To get an intuitive understanding of the Floquet states in the site basis without too many different parameters, let us consider the case of exact resonance, i.e. $\Delta \to 0$. In this case, only zero-th order terms in $H_{\text{vib},\mathscr{E},mn}/\omega$ contribute to the transport in the energy basis as shown above. Therefore, only zero-th order terms in $H_{\text{vib},\mathscr{E},mn}/\omega$ will contribute to transport in the site basis. The Floquet states in the site basis can thus be written in terms of the 'resonant' Floquet states in the energy basis, truncated down to only zero-th order terms in $H_{\text{vib},\mathscr{E},mn}/\omega$:

$$|\phi_1(t)\rangle_{\text{res}} = \frac{1}{\sqrt{2}}\begin{pmatrix} 1e^{-i\frac{\omega}{2}t} \\ 0 \\ ie^{i\frac{\omega}{2}t} \end{pmatrix}_{\mathscr{E}}, \quad |\phi_2(t)\rangle_{\text{res}} = \begin{pmatrix} 0 \\ 1 \\ 0 \end{pmatrix}_{\mathscr{E}}, \quad |\phi_3(t)\rangle_{\text{res}} = \frac{1}{\sqrt{2}}\begin{pmatrix} ie^{-i\frac{\omega}{2}t} \\ 0 \\ 1e^{i\frac{\omega}{2}t} \end{pmatrix}_{\mathscr{E}}. \tag{III.50}$$

Substituting into Eq. (III.49) and keeping terms up to second order in v, the Floquet states

expressed in the site basis are found to be

$$|\phi_1(t)\rangle_{\text{res}} = \frac{1}{\sqrt{2}} \begin{pmatrix} e^{-i\frac{\omega}{2}t} - v^2 \frac{1+i}{2} \left(\cos\left(\frac{\omega}{2}t\right) - \sin\left(\frac{\omega}{2}t\right)\right) \\ v(1+i)\left(\cos\left(\frac{\omega}{2}t\right) - \sin\left(\frac{\omega}{2}t\right)\right) \\ ie^{i\frac{\omega}{2}t} - v^2 \frac{1+i}{2} \left(\cos\left(\frac{\omega}{2}t\right) - \sin\left(\frac{\omega}{2}t\right)\right) \end{pmatrix}_{\mathscr{B}},$$

$$|\phi_2(t)\rangle_{\text{res}} = \frac{1}{\sqrt{2}} \begin{pmatrix} -v \\ 1-v^2 \\ -v \end{pmatrix}_{\mathscr{B}}, \tag{III.51}$$

$$|\phi_3(t)\rangle_{\text{res}} = \frac{1}{\sqrt{2}} \begin{pmatrix} ie^{-i\frac{\omega}{2}t} - v^2 \frac{1+i}{2} \left(\cos\left(\frac{\omega}{2}t\right) + \sin\left(\frac{\omega}{2}t\right)\right) \\ v(1+i)\left(\cos\left(\frac{\omega}{2}t\right) + \sin\left(\frac{\omega}{2}t\right)\right) \\ e^{i\frac{\omega}{2}t} - v^2 \frac{1+i}{2} \left(\cos\left(\frac{\omega}{2}t\right) + \sin\left(\frac{\omega}{2}t\right)\right) \end{pmatrix}_{\mathscr{B}},$$

with corresponding 'resonant' quasi-energies unchanged by the basis transformation:

$$\varepsilon_{1,\text{res}} = c, \quad \varepsilon_{2,\text{ res}} = 0, \quad \varepsilon_{3,\text{ res}} = -c. \tag{III.52}$$

Comparing the form of the 'resonant' Floquet states in the site and energy bases, it can be seen that the basis transformation effectively 'leaks' terms of order v and v^2 from one component to another.

Now, transport in the site basis can be calculated. The transfer probability from the input to the output site, $\mathscr{P}(t,t_0)$, as a function of time t with initial condition $|\psi(t=t_0)\rangle = |\text{in}\rangle$ is given by

$$\begin{aligned}
\mathscr{P}(t,t_0) &= \left|\langle \text{out}|\psi(t,t_0)\rangle\right|^2 \\
&= \left|\sum_{i=1}^{3} e^{-i\varepsilon_i(t-t_0)} \langle \text{out}|\phi_i(t)\rangle \langle \phi_i(t_0)|\text{in}\rangle\right|^2 \\
&= \left|e^{-i\varepsilon_1(t-t_0)} \langle \text{out}|\phi_1(t)\rangle \langle \phi_1(t_0)|\text{in}\rangle + v^2 + e^{-i(-\varepsilon_1)(t-t_0)} \langle \text{out}|\phi_3(t)\rangle \langle \phi_3(t_0)|\text{in}\rangle\right|^2 \\
&= \left|\frac{1}{2}e^{-ic(t-t_0)}\left[ie^{i\frac{\omega}{2}(t+t_0)} + v^2 Q(t,t_0)\right] + v^2 - \frac{1}{2}e^{ic(t-t_0)}\left[ie^{i\frac{\omega}{2}(t+t_0)} + v^2 R(t,t_0)\right]\right|^2 \\
&= \frac{1}{2}\Big(1 - \cos\left[2c(t-t_0)\right]\Big) + v^2 \sin\left[c(t-t_0)\right] S(t,t_0),
\end{aligned} \tag{III.53}$$

where the oscillating functions $Q(t,t_0)$, $R(t,t_0)$ and $S(t,t_0)$ are defined by

$$\begin{aligned}
Q(t,t_0) &:= -\frac{1+i}{2}\left[e^{i\frac{\omega}{2}t}\left(\cos\left(\frac{\omega}{2}t_0\right) - \sin\left(\frac{\omega}{2}t_0\right)\right) + e^{i\frac{\omega}{2}t_0}\left(\cos\left(\frac{\omega}{2}t\right) - \sin\left(\frac{\omega}{2}t\right)\right)\right], \\
R(t,t_0) &:= -\frac{1-i}{2}\left[e^{i\frac{\omega}{2}t}\left(\cos\left(\frac{\omega}{2}t_0\right) + \sin\left(\frac{\omega}{2}t_0\right)\right) + e^{i\frac{\omega}{2}t_0}\left(\cos\left(\frac{\omega}{2}t\right) + \sin\left(\frac{\omega}{2}t\right)\right)\right],
\end{aligned} \tag{III.54}$$

$$S(t,t_0) := \Big\{ \cos\Big[c(t-t_0)+\frac{\omega}{2}(t+t_0)\Big]\mathscr{R}[Q(t,t_0)] + \sin\Big[c(t-t_0)+\frac{\omega}{2}(t+t_0)\Big]\mathscr{I}[Q(t,t_0)] \\ + \cos\Big[c(t-t_0)-\frac{\omega}{2}(t+t_0)\Big]\mathscr{R}[R(t,t_0)] - \sin\Big[c(t-t_0)-\frac{\omega}{2}(t+t_0)\Big]\mathscr{I}[R(t,t_0)] \\ + 2\cos\big[\frac{\omega}{2}(t+t_0)\big]\Big\}. \tag{III.55}$$

The transfer probability at exact resonance has a dominant $(1-\cos[2c(t-t_0)])/2$ term identical to the sinusoidal oscillation found for transport in the energy basis at exact resonance (Eq. (III.48)). This oscillation is then garnished by small oscillations of amplitude v^2 and frequency $\omega/2$. To see the effect of the small rapid oscillations on the overall sinusoidal transport oscillation, a graph of the analytical solution for $\mathscr{P}(t,t_0)$ is plotted using *Mathematica* and is shown in Fig. III.3.

To check the accuracy of the analytical solution, a numerical solution for $\big|\langle \text{out}|\psi(t,t_0=0)\rangle\big|^2$ of the same Hamiltonian is plotted in *Python* (using a numerical ODE solver) and is shown in Fig. III.4. For completeness, numerical solutions for the probability of transporting to the intermediate (mid) site $\big|\langle \text{mid}|\psi(t,t_0=0)\rangle\big|^2$ and the probability of staying in the input site $\big|\langle \text{in}|\psi(t,t_0=0)\rangle\big|^2$ are also plotted on the same graph. A striking similarity between the analytical and numerical solutions is seen, with only small deviations found when taking a zoomed-in view of the rapid small oscillations. This provides numerical evidence that the extensive Floquet and perturbation theory calculations carried out above are valid and correct.

The transfer time for this three-site system occurs at approximately

$$\tau_{\text{3-site}} = \frac{\pi}{2|c|}, \tag{III.56}$$

which is consistent with the two-site result of Eq. (II.68) from [4].

III.2.2 Generalisation to an N-site Hamiltonian

Having analytically calculated the transfer probability for a three-site Hamiltonian, let us consider how the results could be generalised to a network of N sites. For a general Floquet-antisymmetric Hamiltonian of more than three sites, analytic calculations become exceedingly complex. Nevertheless, results obtained in the 3×3 case can be qualitatively generalised and compared to numerical simulations.

Given that only transport between the input and output sites is of interest, the intermediate sites of an N-site network can be effectively treated as a single intermediate site in a three-site network. With more sites, the dimension of the Hilbert space increases and each Floquet state can be represented by an N-dimensional vector in $\mathscr{H}=\mathbb{C}^N$. The frequency of the small rapid oscillations in Eq. (III.53) is given by $\omega/2\approx E$, which is the only independent matrix element of $H_{\text{static},\mathscr{E}}$. Thus, the overall oscillation in the N-site case would be expected to be garnished by many more rapidly oscillating terms of various frequencies, determined by the matrix el-

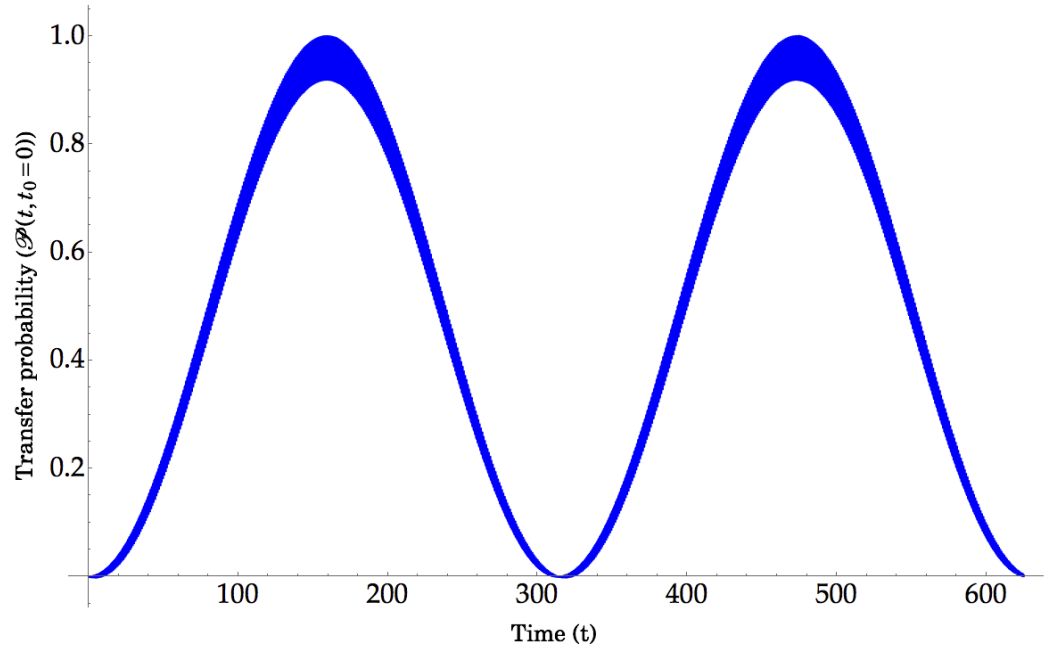

(a)

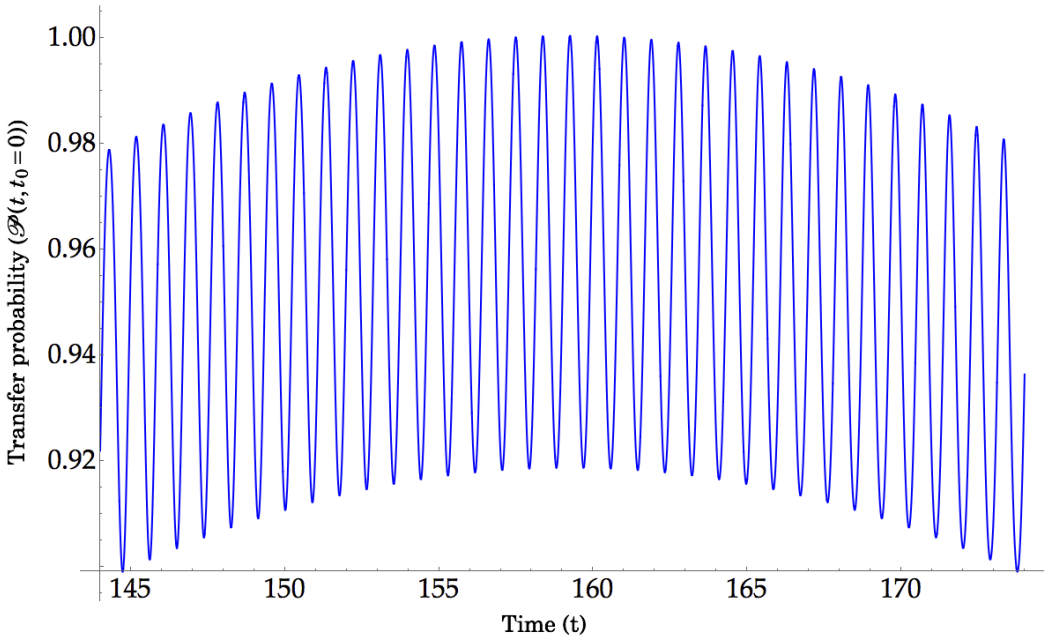

(b)

Figure III.3: A plot of the transfer probability $\mathscr{P}(t, t_0) = \left|\langle \text{out}|\psi(t, t_0 = 0)\rangle\right|^2$ using the analytically calculated expression in Eq. (III.53) for a three-site Floquet-antisymmetric Hamiltonian of the form of Eq. (III.19). (a) shows two periods of oscillation, while (b) shows a zoomed in view of the small rapid oscillations. The parameters chosen are $D = 7,\ V = 1,\ c = 0.01,\ t_0 = 0,\ \omega = \omega_0 = 2E$ (arbitrary units).

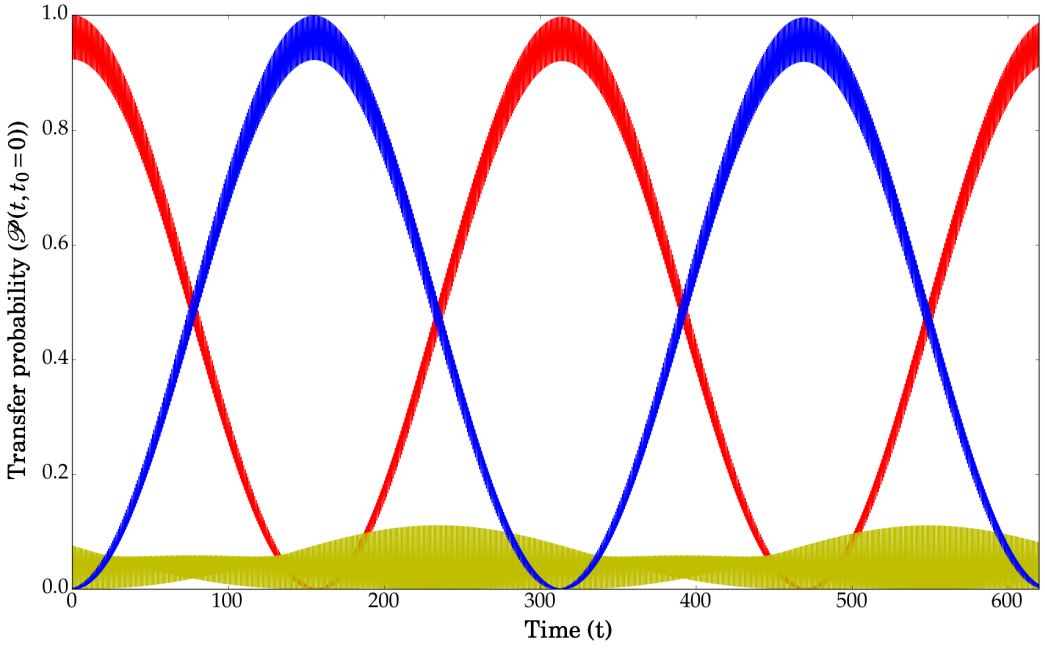

(a)

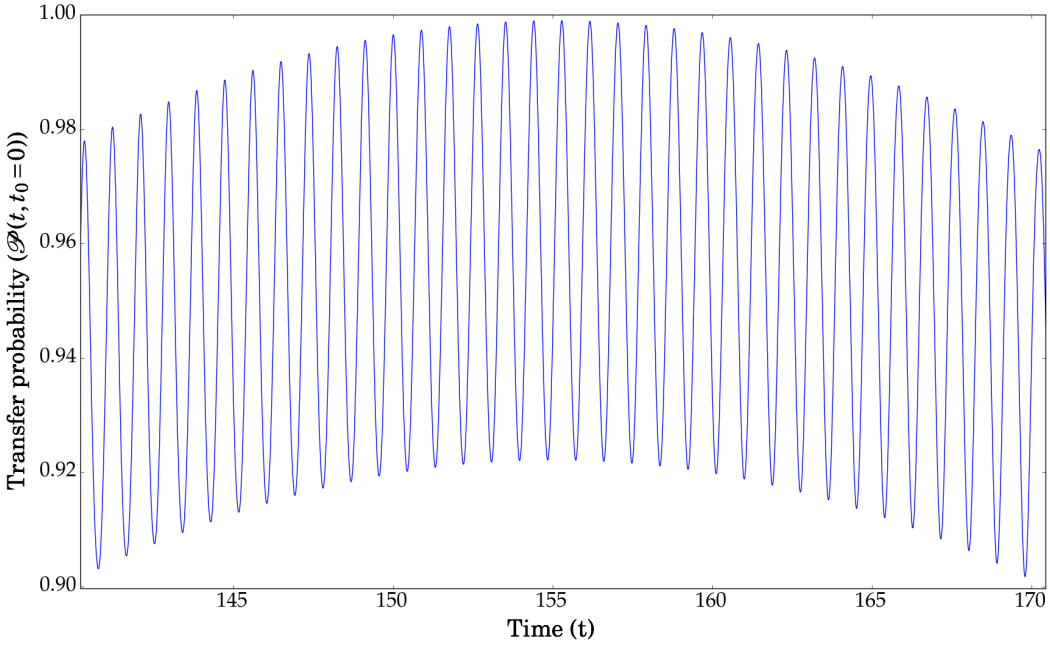

(b)

Figure III.4: A plot of the transfer probability $\mathscr{P}(t, t_0) = \left|\langle \text{out}|\psi(t, t_0 = 0)\rangle\right|^2$ (blue), the probability of transporting to the intermediate site $\left|\langle \text{mid}|\psi(t, t_0 = 0)\rangle\right|^2$ (yellow) and the probability of staying in the input site $\left|\langle \text{in}|\psi(t, t_0 = 0)\rangle\right|^2$ (red), using a numerical ODE solver for a three-site Floquet-antisymmetric Hamiltonian of the form of Eq. (III.19). (a) shows two periods of oscillation, while (b) shows a zoomed in view of the small rapid oscillations. The parameters chosen are $D = 7$, $V = 1$, $a = b = c = d = 0.01$, $t_0 = 0$, $\omega = \omega_0 = 2E$ (arbitrary units).

ements of $H_{\text{static},\mathscr{E}}$. Furthermore, statistics start playing a role: with more elements of the Hamiltonian it no longer makes sense to consider solutions for specific parameters, but rather the Hamiltonian elements need to be picked from their respective distributions as specified in § II.1.

To get a feeling for the transfer probability in the N-site case, numerical solutions for the transfer probability for two representative realisations of the N-site Hamiltonian of the form of Eq. (III.14) are plotted in Fig. III.5 – one exhibiting efficient transport and another one exhibiting suboptimal transport.

Returning to the primary aim of this work, namely generalising the design principles of *centrosymmetry* and *dominant doublet* from a static Hamiltonian to a time-periodic one, a solution for the latter can be found by investigating the Floquet states of those N-site Hamiltonians which do exhibit efficient transport.

III.3 Dominant Floquet doublet

The second aim of this work is to generalise the *dominant doublet* design principle for a static Hamiltonian, a condition on the Hamiltonian eigenvectors, to a time-periodic Hamiltonian.

III.3.1 Formulation of the condition

In the static case, the dominant doublet condition was defined with respect to the eigenvectors of an idealised two-site Hamiltonian which exhibits perfect transport: $|\pm\rangle = (|\text{in}\rangle \pm |\text{out}\rangle)/\sqrt{2}$. Specifically, it states that if a static Hamiltonian has two eigenvectors which are similar to $|\pm\rangle$ (as mathematically formulated in Eq. (II.55)), then the maximum transfer probability will be close to 1. For the time-periodic case, having found analogously ideal *Floquet states* $|\phi_i(t)\rangle_{\text{res}}$ for the 3×3 case in Eq. (III.50), I propose a *dominant Floquet doublet* (DFD) condition for the Floquet states, analogously defined in terms of overlap with the ideal Floquet states.

To this end, the ideal Floquet states in $\mathbb{C}^N$ are defined as

$$\begin{aligned} |+(t)\rangle &:= \frac{1}{\sqrt{2}}(e^{-i\frac{\omega}{2}t}|\text{in}\rangle + ie^{i\frac{\omega}{2}t}|\text{out}\rangle), \\ |-(t)\rangle &:= \frac{1}{\sqrt{2}}(ie^{-i\frac{\omega}{2}t}|\text{in}\rangle + e^{i\frac{\omega}{2}t}|\text{out}\rangle), \end{aligned} \tag{III.57}$$

where the notation $|\pm(t)\rangle$ is used to emphasise the analogy to the static case. The explicit t-dependence of the states avoids confusion with the static $|\pm\rangle$ states. Note that

$$\begin{aligned} |+\ (t=-\pi/(2\omega))\rangle &= e^{i\frac{\pi}{4}}|+\rangle\,, \\ |-\ (t=\pi/(2\omega))\rangle &= e^{i\frac{\pi}{4}}|-\rangle\,, \end{aligned} \tag{III.58}$$

i.e. there exist times $t_\pm$ for which each of the $|\pm(t)\rangle$ states are equal to the $|\pm\rangle$ states up to a

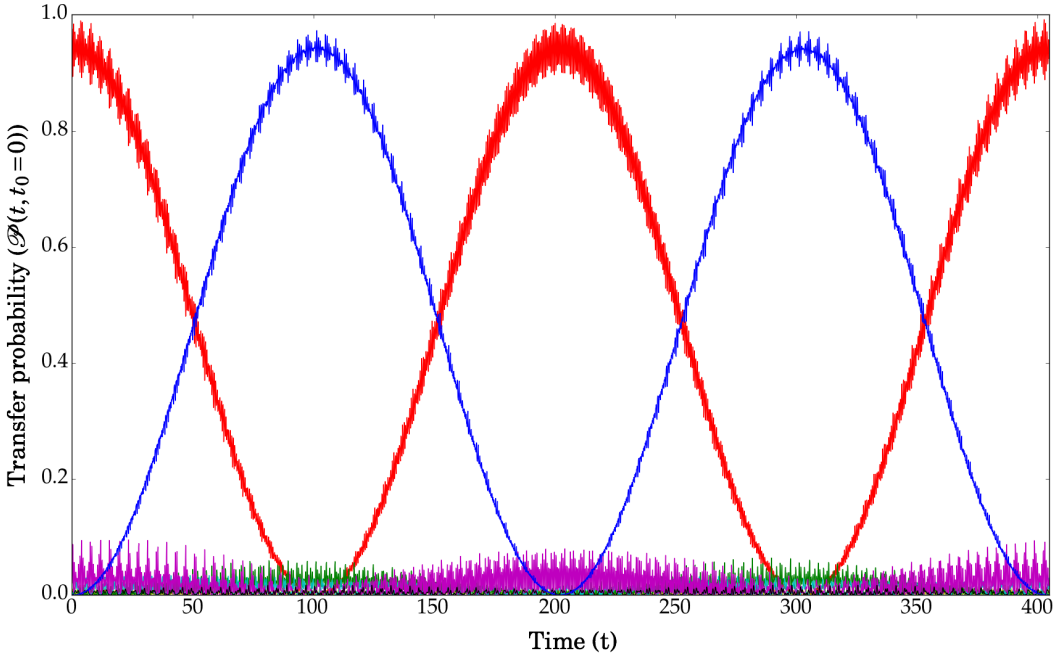

(a)

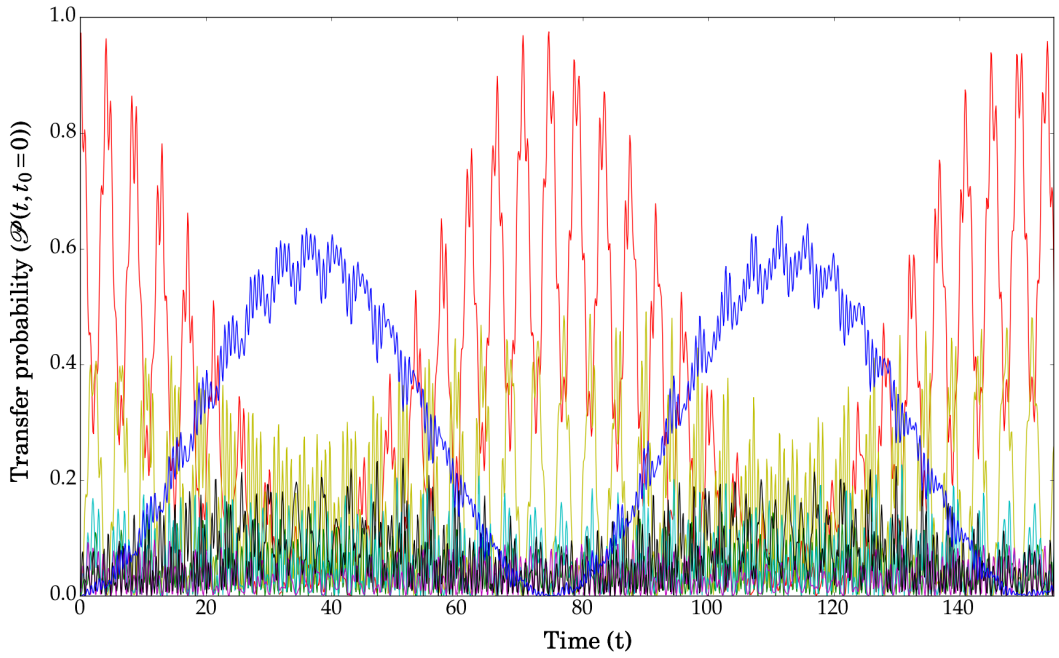

(b)

Figure III.5: A plot of the transfer probability $\mathscr{P}(t, t_0) = \left|\langle \text{out}|\psi(t, t_0 = 0)\rangle\right|^2$ (blue), the probability of staying in the input site $\left|\langle \text{in}|\psi(t, t_0 = 0)\rangle\right|^2$ (red) and the probability of transporting to the other intermediate sites (other colours) in a seven-site network, using a numerical ODE solver for two Floquet-antisymmetric Hamiltonian of the form of Eq. (III.14), at exact resonance. (a) shows a realisation exhibiting reasonably good transport, whilst (b) depicts a suboptimal realisation. The parameters of the statical distributions as defined in § II.1 are $\xi = \eta = 1$, $D_0 = 10$, $\sigma = 0.02$ (arbitrary units).

global phase [27]. Although the $|\pm(t)\rangle$ states have phase factors with frequency $\omega/2$, they are effectively ω-periodic because the relative phase between their $|\text{in}\rangle$ and $|\text{out}\rangle$ components is ω.

Rearranging the expressions, the $|\text{in}\rangle$ and $|\text{out}\rangle$ states can be expanded in terms of the $|\pm(t)\rangle$ states:

$$\begin{aligned} |\text{in}\rangle &= \frac{1}{\sqrt{2}} e^{i\frac{\omega}{2}t}(|+(t)\rangle - i\,|-(t)\rangle), \\ |\text{out}\rangle &= \frac{1}{\sqrt{2}} e^{-i\frac{\omega}{2}t}(-i\,|+(t)\rangle + |-(t)\rangle). \end{aligned} \tag{III.59}$$

The $|\pm(t)\rangle$ are seen to obey orthonormality at each time t and are related by a $\hat{P}$-symmetry:

$$\langle +(t)|+(t)\rangle = \langle -(t)|-(t)\rangle = 1, \quad \langle +(t)|-(t)\rangle = 0, \quad \forall t, \tag{III.60}$$

$$\hat{P}\,|\pm(t)\rangle = |\mp(t)\rangle\,. \tag{III.61}$$

In formulating the condition, Floquet states are desired to be 'similar' to the $|\pm(t)\rangle$ states. In the static case, this could be simply formulated in terms of the modulus squared of the overlap between the Hamiltonian eigenstates and the $|\pm\rangle$ states (Eq. (II.55)). For the case of the Floquet states, the time-dependence must be taken into account in some way, because high overlap at one point in time does not automatically ensure high overlap at all other times. One approach would be to say that the Floquet states require high overlap with $|\pm(t)\rangle$ at *all* points in time; however this is very restrictive as it would exclude Floquet states which have almost perfect overlap say 99% of the time within the time period $[0,T)$, if they fall below the given threshold for 1% of the time. Therefore, I propose that the condition is defined in terms of the *mean* modulus squared of the overlap over one time period [7]. This implies that the overlap modulus squared cannot remain far below one for any extended period of time. The condition can be formulated as follows:

Dominant Floquet doublet condition: Let $H(t)$ be a time-periodic Hamiltonian with time period $T = 2\pi/\omega$ on $\mathscr{H} = \mathbb{C}^N$, with a corresponding Floquet Hamiltonian H_F on $\mathscr{H}_\text{F} = \mathbb{C}^N \otimes \text{L}^2\big([0,T)\big)$. Let $\mathscr{F}(H_\text{F})$ be the set of Floquet states of H_F. Then $H(t)$ has a *dominant Floquet doublet* if

$$\exists\,|\phi_+(t)\rangle, |\phi_-(t)\rangle \in \mathscr{F}(H_\text{F}), \text{ such that } 1 \geq \frac{1}{T}\int_0^T \big|\langle\phi_\pm(t)|\pm(t)\rangle\big|^2\,\text{d}t \geq \beta \approx 1. \tag{III.62}$$

III.3.2 Definition of efficient transport in an oscillating network

The figure of merit for efficient quantum transport was defined in Eq. (II.9) to be the maximum transfer probability to the output site, $\mathscr{P}_\text{max}(t_0)$, of an excitation initially localised at the input site at time t_0. For a static network, this was independent of the intial time t_0 at which the excitation arrives at the input site (Eq. (II.4)). However, for the case of a time-periodic network,

the time t_0 is a variable which needs to be considered, as it defines the phase of the oscillations when the excitation enters the network. Nevertheless, the input time t_0 cannot be controlled in general. For example, in the FMO complex, it depends on the time at which a photon is received from the sun. Therefore, for a network to reliably lead to efficient transport, it must have a high maximum transfer probability, on average, for all $t_0 \in [0, T)$.

In order to capture the idea of high $\mathscr{P}_{\max}(t_0)$ *on average* over a time period, I propose a modified, t_0-indepenedent, definition for the maximum transfer probability in an oscillating network:

$$\mathscr{P}_{\max} := \frac{1}{T}\int_0^T \max_{t\in[t_0,t_0+T_{\mathrm{R}})} \underbrace{|\langle \mathrm{out}|\psi(t,t_0)\rangle|^2}_{=\mathscr{P}(t,t_0)} \mathrm{d}t_0, \tag{III.63}$$

with efficient transport occuring for $\mathscr{P}_{\max}$ close to 1. By considering that the transfer probability $\mathscr{P}(t,t_0)$ is bounded between 0 and 1, it can be seen [7] that

$$\mathscr{P}_{\max} = \frac{1}{T}\int_0^T \max_{t\in[t_0,t_0+T_{\mathrm{R}})} \underbrace{|\langle \mathrm{out}|\psi(t,t_0)\rangle|^2}_{=\mathscr{P}(t,t_0)} \mathrm{d}t_0 \geq \max_{t\in[t_0,t_0+T_{\mathrm{R}})} \underbrace{\frac{1}{T}\int_0^T |\langle \mathrm{out}|\psi(t,t_0)\rangle|^2 \mathrm{d}t_0}_{=:\mathscr{P}(t)}, \tag{III.64}$$

where $\mathscr{P}(t)$ for a time-periodic network is defined as the transfer probability averaged over t_0.

III.3.3 Transport under the dominant Floquet doublet condition

For a Hamiltonian satisfying the DFD condition, an exact lower bound for $\mathscr{P}_{\max}$ can be calculated, in an analogous way to the lower bound under the static dominant doublet condition, stated in Eq. (II.62). First, a bound for the t_0-averaged transfer probability $\mathscr{P}(t)$ is found. The state of the system $|\psi(t,t_0)\rangle$ is expanded in the Floquet expansion of Eq. (II.14) and the $|\mathrm{in}\rangle$ and $|\mathrm{out}\rangle$ states are expanded in terms of the $|\pm(t)\rangle$ states using Eq. (III.59). A stroboscopic approach is taken, as in the preliminary results presented in Eq. (II.66), where the transfer probability only at times $(t-t_0) = kT,\ k \in \mathbb{N}$ is considered. This, when taken together with the integral over the initial phase, effectively averages over the small rapid oscillations. Thus, taking the Floquet states and quasi-energies of the Hamiltonian to be $|\phi_i(t)\rangle$ and ε_i, respectively,

$$\begin{aligned}\mathscr{P}(t) &= \frac{1}{T}\int_0^T \left|\langle \mathrm{out}|\psi(t,t_0)\rangle\right|^2 \mathrm{d}t_0 \\ &= \frac{1}{T}\int_0^T \left|\sum_{i=1}^{N} e^{-i\varepsilon_i(t-t_0)} \langle \mathrm{out}|\phi_i(t)\rangle \langle \phi_i(t_0)|\mathrm{in}\rangle\right|^2 \mathrm{d}t_0\end{aligned} \tag{III.65}$$

$$\begin{aligned}
\Rightarrow \mathscr{P}(t = t_0 + kT) &= \frac{1}{T}\int_0^T \left| \sum_{i=1}^{N} e^{-i\varepsilon_i kT} \langle \text{out}|\phi_i(t_0)\rangle \langle \phi_i(t_0)|\text{in}\rangle \right|^2 \mathrm{d}t_0 \\
&= \frac{1}{T}\int_0^T \left| \sum_{i=1}^{N} e^{-i\varepsilon_i kT} e^{i\omega t_0} \frac{1}{2}\Big[i|\langle +(t_0)|\phi_i(t_0)\rangle|^2 - i|\langle -(t_0)|\phi_i(t_0)\rangle|^2 \right. \\
&\qquad \left. + \langle +(t_0)|\phi_i(t_0)\rangle \langle \phi_i(t_0)|-(t_0)\rangle + \langle -(t_0)|\phi_i(t_0)\rangle \langle \phi_i(t_0)|+(t_0)\rangle \Big] \right|^2 \mathrm{d}t_0,
\end{aligned} \tag{III.66}$$

where the $i = \pm$ terms have been singled out in the sum.

At this point, the Cauchy-Schwarz inequality [28] can be used. For any two functions $f(t), g(t)$ on $\mathrm{L}^2\big([0,T)\big)$, the Cauchy-Schwarz inequality states that

$$\left| \frac{1}{T}\int_0^T f(t) g^*(t)\,\mathrm{d}t \right|^2 \leq \frac{1}{T}\int_0^T |f(t)|^2\,\mathrm{d}t \; \frac{1}{T}\int_0^T |g(t)|^2\,\mathrm{d}t. \tag{III.67}$$

For $g(t) = 1$ and $f(t)$ equal to the expression inside the outer modulus signs of the right-hand side of Eq. (III.66):

$$\begin{aligned}
\mathscr{P}(t = t_0 + kT) &\geq \left| \frac{1}{T}\int_0^T \sum_{i=1}^{N} \left[\frac{i}{2} e^{-i\varepsilon_i kT} \Big(|\langle +(t_0)|\phi_i(t_0)\rangle|^2 - |\langle -(t_0)|\phi_i(t_0)\rangle|^2 \Big) \right. \right. \\
&\qquad \left. \left. + e^{-i\varepsilon_i kT} \Re\Big[\langle +(t)|\phi_i(t_0)\rangle \langle \phi_i(t_0)|-(t)\rangle \Big] \right] \mathrm{d}t_0 \right|^2 . \\
&= \left| \frac{i}{2} e^{-i\varepsilon_+ kT} \frac{1}{T}\int_0^T |\langle +(t_0)|\phi_+(t_0)\rangle|^2\,\mathrm{d}t_0 - \frac{i}{2} e^{-i\varepsilon_- kT} \frac{1}{T}\int_0^T |\langle -(t_0)|\phi_-(t_0)\rangle|^2\,\mathrm{d}t_0 \right. \\
&\qquad + \sum_{\substack{i=1 \\ i\neq +}}^{N} \frac{i}{2} e^{-i\varepsilon_i kT} \frac{1}{T}\int_0^T |\langle +(t_0)|\phi_i(t_0)\rangle|^2\,\mathrm{d}t_0 - \sum_{\substack{i=1 \\ i\neq -}}^{N} \frac{i}{2} e^{-i\varepsilon_i kT} \frac{1}{T}\int_0^T |\langle -(t_0)|\phi_i(t_0)\rangle|^2\,\mathrm{d}t_0 \\
&\qquad \left. + \sum_{i=1}^{N} e^{-i\varepsilon_i kT} \frac{1}{T}\int_0^T \Re\Big[\langle +(t_0)|\phi_i(t_0)\rangle \langle \phi_i(t_0)|-(t_0)\rangle \Big]\,\mathrm{d}t_0 \right|^2 .
\end{aligned} \tag{III.68}$$

The first two terms on the right-hand side of Eq. (III.68) are large, with moduli larger than the limit set by the dominant Floquet doublet condition in Eq. (III.62), namely $\beta/2$ each. The three additional sums are much smaller and an upper bound for their contribution is derived in the Appendix. The quantity of interest is $\mathscr{P}_{\max}$, which by Eq. (III.64) is larger than the maximum of $\mathscr{P}(t = t_0 + kT)$, assuming an arbitrarily large reference time T_{R}. This maximum occurs when the phase factors of the two large terms align, resulting in a contribution with absolute value greater than β. The combination of this lower bound with the upper bounds on the small terms results in an exact lower bound for $\mathscr{P}(t = t_0 + kT)$ and consequently $\mathscr{P}_{\max}$:

$$\mathscr{P}_{\max} \geq \max_{t\in[t_0, t_0+T_{\mathrm{R}})} \mathscr{P}(t = t_0 + kT) \geq \left| \beta - \Big(1 + \sqrt{N-2}\Big)(1-\beta) - 2\sqrt{1-\beta} \right|^2 . \tag{III.69}$$

For β sufficiently large, and network sizes with N of the order of ten, the right-hand side of

this inequality can be made close to one. Nevertheless, due to the square root term $\sqrt{1-\beta}$ which is large even for small $1-\beta$, β would need to be set as high as 0.9994 in order to ensure $\mathscr{P}_{\max} \geq 0.9$.

It is important to note that the lower bound is an extreme case, and will most often be far from saturation. The three sums consist of small oscillatory terms of various frequencies and could be considered negligible on average (i.e. at each point in time approximately half of the terms will add up and the other half subtract from the large term). This is analogous to the argument for the dominant doublet case in [3]. Then, by analogy to the dominant doublet calculation in Eq. (II.59), an approximate bound for the maximum transfer probability (explicitly incorporating T_{R}) is:

$$\mathscr{P}_{\max} \geq \max_{t\in[t_0,t_0+T_{\mathrm{R}})} \mathscr{P}(t=t_0+kT) \gtrsim \frac{2\beta-1}{2} \max_{t\in[t_0,t_0+T_{\mathrm{R}})} \Big[1-\cos[(\varepsilon_+-\varepsilon_-)kT]\Big]. \tag{III.70}$$

This is reminiscent of the dominant doublet result in Eq. (II.62) for a static Hamiltonian and the dominant Floquet doublet result for the special case of $t_0 = 0$ in Eq. (II.66).

III.3.4 Floquet antisymmetry and the dominant Floquet doublet

In the static case, centrosymmetry both enhanced the probability of obtaining a realisation satisfying the dominant doublet condition and, given a dominant doublet realisation, improved the lower bound for $\mathscr{P}_{\max}$. The former was motivated by Eq. (II.48), a result for centrosymmetric matrices. In the time-periodic case, an analogous, but different, property of Floquet-antisymmetric operators suggests that Floquet-antisymmetry may enhance the probability of obtaining a dominant Floquet doublet realisation. The desirable property for Floquet-antisymmetric operators is a corollary of Eq. (III.18), namely that

$$\begin{aligned} \{H_{\mathrm{F}},\bar{P}\}=0 \Rightarrow \forall\, |\phi_i(t)\rangle \in \mathscr{F}(H_{\mathrm{F}}),\ &\text{with eigenvalue } \varepsilon_i, \\ \exists\, \bar{P}\,|\phi_i(t)\rangle \in \mathscr{F}(H_{\mathrm{F}}),\ &\text{with eigenvalue } -\varepsilon_i. \end{aligned} \tag{III.71}$$

This means that if a Hamiltonian is Floquet antisymmetric, i.e. $\{H_{\mathrm{F}},\bar{P}\}=0$, then the existence of the $|\phi_+(t)\rangle$ state automatically ensures the existence of the $|\phi_-(t)\rangle = \bar{P}\,|\phi_+(t)\rangle$ state, with equal modulus squared of the overlap with $|-(t)\rangle$ as $|\phi_+(t)\rangle$ has with $|+(t)\rangle$. Therefore, the dominant doublet condition of Eq. (II.55) on two Floquet states can be reduced to a condition on one Floquet state:

$$\exists\, |\phi_+(t)\rangle \in \mathscr{F}(H_{\mathrm{F}}),\ \text{such that } 1 \geq \frac{1}{T}\int_0^T \big|\langle\phi_+(t)|+(t)\rangle\big|^2\,\mathrm{d}t \geq \beta \approx 1, \tag{III.72}$$

with the second condition for $|\phi_-(t)\rangle$ automatically satisfied.

Since imposing Floquet antisymmetry on an ensemble reduces the number of requirements for satisfying the dominant Floquet doublet condition, the probability of obtaining a realisa-

tion satisfying the DFD condition is expected to increase under Floquet antisymmetry. To test this hypothesis, I wrote a *Python* program to sample 10000 Hamiltonians from each of two ensembles, one random GOE and another GOE with Floquet-antisymmetry, and compare their dominant Floquet doublet characteristics.

The program begins by sampling Hamiltonians of the form of Eq. (III.14) with the individual terms sampled from their respective distributions as specified in § II.1 (with the distribution of the free parameters of centrosymmetric matrices modified to the form of Eq. (II.49) and anti-centrosymmetric matrices unmodified). It then uses the methods of § II.2.1.c to numerically compute the Floquet states and quasi-energies for each Hamiltonian. The overlap modulus squared of each Floquet state with $|+(t)\rangle$, integrated over a whole period of the vibrational mode, is calculated and the state with the highest overlap squared is then called the $|\phi_+(t)\rangle$ state. The *strength* of the dominant Floquet doublet of each Hamiltonian is denoted β_H and is defined by

$$\beta_H \coloneqq \frac{1}{T}\int_0^T \left|\langle\phi_+(t)|+(t)\rangle\right|^2 \mathrm{d}t. \tag{III.73}$$

The results of the simulations are shown in Fig. III.6. A clear difference in probability of obtaining realisations with $\beta_H \geq 0.9$ is seen between the two ensembles, with the Floquet-antisymmetric ensemble greatly superior in this respect (13% compared to 5%). This numerically supports the argument above that Floquet-antisymmetry increases the probability of obtaining DFD realisations and also explains the numerical results of §III.1.5 that realisations with high maximum transfer probability are more likely to occur in Floquet-antisymmetric ensembles.

Now considering transport under a Hamiltonian satisfying both Floquet antisymmetry and the DFD condition, the symmetry properties of the Floquet states and quasi-energies in Eq. (III.71) lead to additional simplifications of the bound for the transfer probability. Here, the number of sites N is taken to be even to simplify the calculations; an analogous result can be found for odd N. All the sums of N exponential terms can then be simplified to sums of $N/2$ sine or cosine terms. Thus, Eq. (III.68) simplifies to

$$\begin{aligned}\mathscr{P}(t = t_0+kT) \geq \Bigg| &\sin(\varepsilon_+ kT)\frac{1}{T}\int_0^T |\langle+(t_0)|\phi_+(t_0)\rangle|^2 \,\mathrm{d}t_0 \\ &+ \sum_{\substack{i=1\\ i\neq+}}^{N/2} \sin(\varepsilon_i kT)\frac{1}{T}\int_0^T |\langle+(t_0)|\phi_i(t_0)\rangle|^2 \,\mathrm{d}t_0 - \sum_{i=1}^{N/2} \sin(\varepsilon_i kT)\frac{1}{T}\int_0^T |\langle-(t_0)|\phi_i(t_0)\rangle|^2 \,\mathrm{d}t_0 \\ &+ \sum_{i=1}^{N/2} 2\cos(\varepsilon_i kT)\frac{1}{T}\int_0^T \Re\Big[\,\langle+(t_0)|\phi_i(t_0)\rangle\,\langle\phi_i(t_0)|-(t_0)\rangle\,\Big]\,\mathrm{d}t_0\Bigg|^2,\end{aligned} \tag{III.74}$$

where the remaining sum over $N/2$ states is arbitrarily chosen to include the $i = +$ but not the

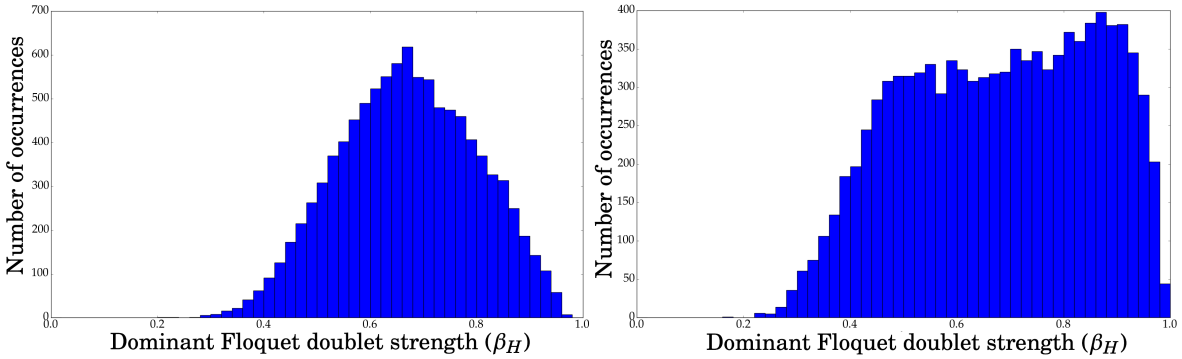

Figure III.6: Histograms showing the distribution of β_H for 10000 time-periodic Hamiltonians of the form of Eq. (II.7) from two different ensembles. (a) depicts the results from a random GOE ensemble with the individual terms of the Hamiltonian taken of the forms defined in § II.1 with parameters $\xi = \eta = 1,\ D_0 = 10,\ \sigma = 0.02,\ N = 8$ (arbitrary units). (b) depicts the results from a random GOE ensemble with Floquet-antisymmetry imposed as defined in Eq. (III.14). The statistical parameters for the remaining independent variables are the same as in (a). Note that the vertical axes on the two plots have been scaled independently to their respective maximum values.

$i = -$ Floquet state. However, unlike centrosymmetry, Floquet antisymmetry does not cancel out the cross terms in the last sum to increase the exact lower bound for $\mathscr{P}_{\max}$. The approximate bound (III.70) for $\mathscr{P}_{\max}$ simplifies to

$$\mathscr{P}_{\max} \geq \max_{t\in[t_0,t_0+T_{\mathrm{R}})} \mathscr{P}(t = t_0+kT) \gtrsim \frac{2\beta-1}{2} \max_{t\in[t_0,t_0+T_{\mathrm{R}})} \Big[1-\cos[2\varepsilon_+ kT]\Big]. \tag{III.75}$$

From this result, it can be seen that the transfer time occurs at approximately

$$\tau_{N\text{-site}} = \frac{\pi}{2|\varepsilon_+|}, \tag{III.76}$$

which is consistent with result in Eq. (II.67) for the transfer time under the special DFD condition with $t_0 = 0$ studied in [4]. Note that as for the special DFD condition, this result for the transfer time relies on the existence of a k such that the sinusoidal oscillation reaches its maximum value in the first oscillation period. The result in [4] that this condition holds is also valid here for Eq. (III.75), under the same assumptions as outlined in § II.3.2.

III.3.5 Statistical investigation of the dominant Floquet doublet bound

To investigate the validity of the approximate bound of Eq. (III.75), a statistical investigation of randomly sampled Floquet-antisymmetric Hamiltonians satisfying the DFD condition was conducted. To this end, I used the *Python* program described in the previous section to sample

random Floquet-antisymmetric GOE Hamiltonians until 1000 Hamiltonians also satisfying the DFD condition with $\beta = 0.95$ were found. The program then numerically computed the dominant doublet strength β_H and the maximum transfer probability $\mathscr{P}_{\max}$ of each Hamiltonian (assuming an arbitrarily long T_{R}). A scatter plot of β_H against $\mathscr{P}_{\max}$ was then plotted along with the approximate bound of Eq. (III.75). The results are shown in Fig. III.7.

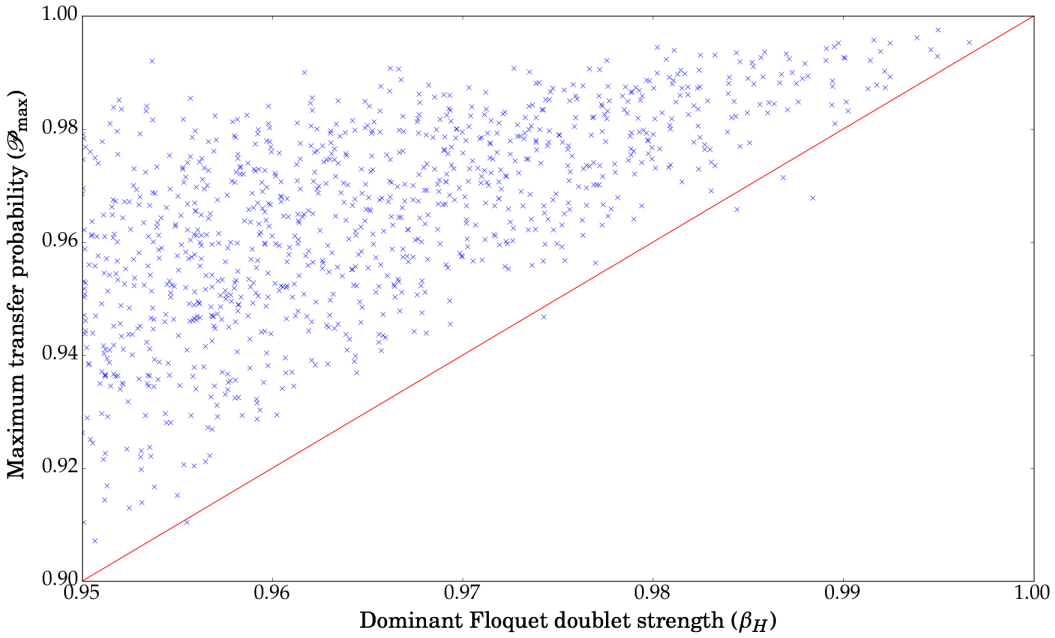

Figure III.7: A scatter plot of the maximum transfer probability $\mathscr{P}_{\max}$ against the dominant Floquet doublet strength β_H for 1000 Floquet-antisymmetric Hamiltonians with $\beta_H > 0.95$ of the form of Eq. (III.14), where each term is given by the distributions described in § II.1 with the parameters $\xi = \eta = 1$, $D_0 = 10$, $\sigma = 0.02$, $N = 8$ (arbitrary units). T_{R} is taken to be arbitrarily large. The red line shows the approximate lower bound of Eq. (III.75), namely $\mathscr{P}_{\max} = 2\beta_H - 1$. The graph shows five realisations violating the approximate bound; two additional points $(0.964, 0.618)$ and $(0.950, 0.163)$ were found to violate the bound but are beyond the limits of the axes.

The scatter plot shows that the approximate bound of Eq. (III.75) is violated by seven of the 1000 realisations sampled. Those seven, however, all satisfy the exact DFD bound of Eq. (III.69). Given that 99.3% of the realisations sampled satisfy the approximate bound, the simulation provides statistical evidence that Eq. (III.75) is an accurate approximate lower bound for the maximum transfer probability of Floquet-antisymmetric Hamiltonians satisfying the dominant Floquet doublet condition.

III.4 Statistics of transfer times

In this final section of Results, a short investigation is presented on the statistics of transfer times for Hamiltonians satisfying the two design principles of Floquet-antisymmetry and dominant Floquet doublet. The approach taken is directly analogous to that followed in the static case [3].

First, an appropriate way of defining the transfer time must be found. In § II.1, the transfer time τ was defined as the time at which the first maximum in transfer probability $\mathscr{P}_{\max}$ occurs. However, for the statistical investigation, each Hamiltonian has a different $\mathscr{P}_{\max}$. Hence, simply comparing the times at which $\mathscr{P}_{\max}$ for each Hamiltonian occurs, would not be comparing like with like. Instead, in line with the thinking behind the dominant Floquet doublet design principle, it makes sense to take a minimum bound γ for $\mathscr{P}_{\max}$, which is considered 'good enough' for efficient transport. A fair comparison can then be made between all the Hamiltonians in investigating the time taken for the transfer probability of each realisation to first reach γ, which will be denoted by τ_γ. If this bound is set to $\gamma = 2\beta - 1$ for an ensemble satisfying the dominant Floquet doublet condition with parameter β, then from Eq. (III.75), (almost) all the Hamiltonians of the ensemble result in $\mathscr{P}_{\max}$ greater than γ.

Note that in contrast to the static case, $\mathscr{P}_{\max}$ for a time-periodic Hamiltonian is defined in § III.3.2 to include an average over all initial phases t_0 within a time period T. Therefore, the transfer times τ and τ_γ should in principle also be the average over a time period of the physical transfer times with initial phase t_0. However, for the purpose of efficient simulations, for each realisation a random initial time t_0 was picked in the interval $[0, T)$ for calculating τ_γ. This allowed far more realisations to be sampled than if the integration had been performed, and the effects of randomly picking t_0 should average out over the sample.

Given that each Hamiltonian is sampled from a random ensemble, the transfer time of each Hamiltonian needs to be scaled with respect to the transfer time of the corresponding two-site system (i.e. with the intermediate sites removed), $\tau_{2\text{-site}}$. An expression for this two-site transfer time is given by Eq. (II.68), and depends on the direct vibrational coupling between the input and output sites.

The statistical investigation was conducted as follows. The minimum bound γ was set to 0.9. Hamiltonians were sampled from a Floquet-antisymmetric GOE ensemble as in the previous sections until 10000 Hamiltonians satisfying the dominant Floquet doublet condition with $\beta = 0.95$ were found. For each of these Hamiltonians, τ_γ was computed for a random t_0. Analogously to the static case (§ II.3.1.c), a histogram of the inverse scaled transfer times $\tau_{2\text{-site}}/\tau_\gamma$ was plotted. The result is shown in Fig. III.8.

The figure shows a sharp peak in the distribution of $\tau_{2\text{-site}}/\tau_\gamma$ centred between 1.0 and 1.1, with a long tail stretching out to the right. This is very much reminiscent of the distribution of scaled inverse transfer times for the static case (§ II.3.1.c), and notably has the peak at the same

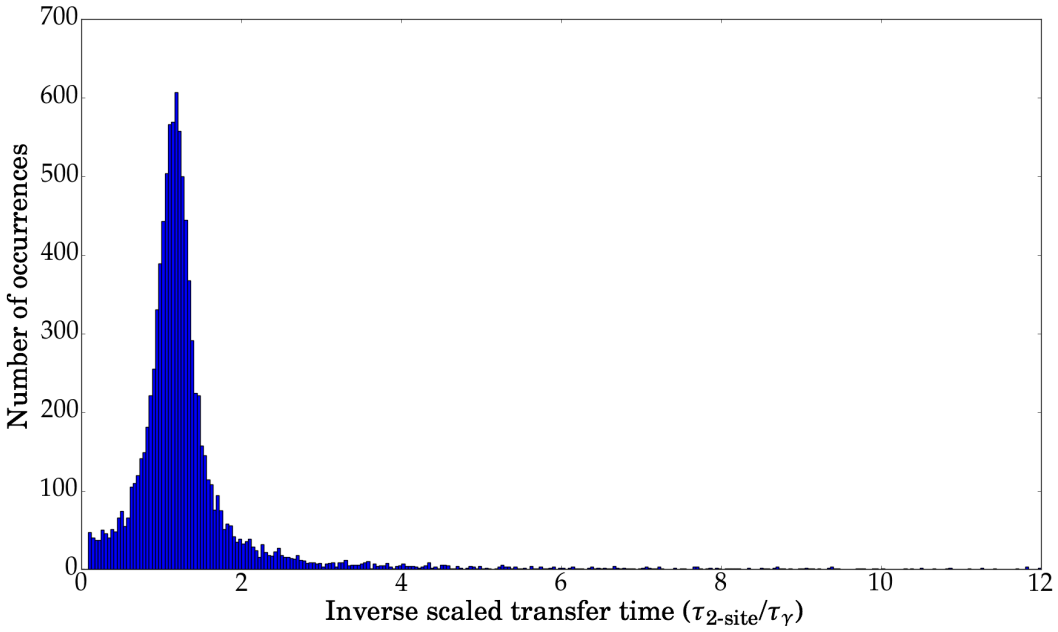

Figure III.8: Histogram showing the distribution of inverse scaled transfer times $\tau_{2\text{-site}}/\tau_\gamma$ for 10000 Hamiltonians satisfying the dominant Floquet doublet condition with $\beta = 0.95$ post-selected from a Floquet-antisymmetric GOE ensemble. The parameters of the different terms of the Hamiltonian (as defined in § II.1) are $\xi = \eta = 1$, $D_0 = 10$, $\sigma = 0.02$, $N = 8$ (arbitrary units). The initial phase $t_0 \in [0, T)$ was sampled from a uniform distribution in $[0, T)$.

place. Analogously, it shows that there exists a non-negligible proportion of realisations with transfer times much faster than those which would occur in the absence of intermediate sites. Specifically, 2.1% of the realisations exhibit transfer times over five times faster than the corresponding two-site systems. Therefore, the third and final aim of this work has been achieved: an ensemble of Hamiltonians satisfying two general design principles has been shown to guarantee high maximum transfer efficiency between the input and output sites, with a significant proportion of these maxima occurring at transfer times much faster than the corresponding times that would occur in the absence of an intermediate network.

Chapter IV

Discussions and Conclusion

This chapter begins by discussing the results of Chapter III in a broader physical context. Applications of the results to biological systems such as the FMO complex as well as to other fields are outlined. Outlook for further research is given where appropriate and the chapter concludes with a summary of the thesis.

IV.1 Remarks and relation to past and future work

At the end of Chapter II, three open problems from previous work were identified. Solutions to each of the three problems were proposed in Chapter III, backed up by detailed calculations and numerical simulations. Let us now take a step back to review the proposed solutions of Chapter III in the context of the previous results presented in § II.3, with emphasis on their relevance, physical consequences and link to potential future work.

IV.1.1 Physical implementation of Floquet antisymmetry

The first design principle found for the static model in [3] was centrosymmetry of the Hamiltonian (defined in Eq. (II.40) and (II.42)). In physical terms, this means that the network appears the same when viewed from the point of view of the input and the output sites. For example, the coupling between sites 1 and 3 is equal to the coupling between sites N and $(N-2)$, i.e. $V_{13} = V_{N,N-2}$, and the on-site energy of site 2 is equal to that of site $(N-1)$, i.e. $E_2 = E_{N-1}$.

Here, the design principle of Floquet antisymmetry is proposed (Eq. (III.9) and (III.13)), which provides a different physical picture. To satisfy this constraint, the static part of the Hamiltonian H_{static} was chosen to be anti-centrosymmetric, while the vibrational part H_{vib} was chosen to be centrosymmetric. But what does this mean for the physical couplings and on-site energies? From the definition of anti-centrosymmetry in Eq. (III.1), an anti-centrosymmetric Hamiltonian is antisymmetric across its secondary diagonal. This means that the static couplings between, for example, sites 1 and 3 and sites N and $(N-2)$ are equal and opposite,

namely $V_{13} = -V_{N,N-2}$. Similarly, the on-site energies come in equal and opposite pairs, e.g. $E_2 = -E_{N-1}$. The case of the energies is easy to understand physically. However, the task of constructing a 3D network with inter-site (dipole-dipole) couplings between all the sites satisfying anti-centrosymmetry is a problem requiring further research.

Moving on to centrosymmetry of the vibrational coupling amplitudes, this symmetry condition is tantamount to imposing that the coupling strength between the network and its environment exhibits a reflection symmetry between the input and output points of view. The couplings to the environment are expected to result from the geometrical structure of the network, so a centrosymmetric coupling landscape suggests a centrosymmetric structure. Both centrosymmetry and anti-centrosymmetry require some sort of reflection symmetry which would be expected to be encoded in the geometrical structure of the network. Finding out exactly how these symmetries can be implemented (with the correct signs) in a physical system (e.g. molecular dipoles in the FMO complex) is an interesting subject for further work.

IV.1.2 Significance of the Floquet solution for a three-site Hamiltonian

In the seminal PhD thesis of Shirley [6], the Floquet formalism was used to analytically (albeit perturbatively) solve the Schrödinger equation for a 2×2 Hamiltonian with static diagonal elements and periodic driving of the off-diagonal elements. The method was also applied to larger Hamiltonians, which under certain conditions could be reduced to the 2×2 case. The Floquet methods greatly improved upon previous solutions using the so called 'rotating wave approximation'.

In the current thesis, Shirley's approach is extended to a 3×3 Hamiltonian under periodic driving, with all elements containing both static and time-periodic terms. This time, the goal was not simply to solve the Schrödinger equation but to calculate, and optimise, the transfer probability between sites 1 and 3. First, a basis transformation was carried out to the energy basis, where the static part of the Hamiltonian is entirely diagonal, such that the methods of Shirley could be used. It was shown that under the proposed Floquet-antisymmetry, the 3×3 case reduces to an effective 2×2 problem, resulting in perfect transport between the highest and lowest energy eigenstates at exact resonance. Transforming back to the site basis, i.e. including the effects of the non-diagonal static terms of the Hamiltonian, transport between the physical sites was calculated. Here it was shown that for small static off-diagonal terms, transport between the input and output sites resembles transport between the highest and lowest energy eigenstates, garnished by small oscillations.

The Floquet calculation presented here provides a solution to a completely general quantum mechanical problem. It incorporates a general Hamiltonian with both static and time-periodic terms, with no constraints on either the diagonal or non-diagonal elements being static or oscillating. This means that the calculation is basis independent, making it more general than the original calculation presented by Shirley. Thus, the results presented here may prove useful

in many other problems in quantum mechanics where an analytical solution for a general time-periodic Hamiltonian is required.

IV.1.3 Interpretation of the dominant Floquet doublet

In [1], the dominant doublet design principle was proposed as a condition on the eigenvectors of a static Hamiltonian which guarantees efficient transport. The mathematical formulation of the condition in Eq. (II.55) effectively says that the Hamiltonian must have two eigenvectors that are close to an equal superposition of the $|\text{in}\rangle$ and $|\text{out}\rangle$ states. For real eigenvectors, this means that the eigenvectors must be similar to either of the $|\pm\rangle = (|\text{in}\rangle \pm |\text{out}\rangle)/\sqrt{2}$ states. If the condition is satisfied, the expression for the transfer probability in Eq. (II.59) is dominated by these two eigenvectors, enabling the transfer probability to reach a maximum close to 1.

The dominant Floquet doublet design principle proposed in this thesis is an analogous condition on the Floquet eigenstates of an abstract Floquet Hamiltonian. These Floquet states can however be interpreted as time-periodic 'eigenvectors' of the physical Hamiltonian, in which case a concrete analogy to the static case can be seen. The Floquet theorem of Eq. (II.14) enables the state of a time-periodic system to be expanded in terms of the Floquet states and corresponding quasi-energies in the same way as the standard eigenvector expansion under a static Hamiltonian. Thus, in the calculation of the transfer probability $\mathscr{P}(t)$ in Eq. (III.66), the Floquet states play the same role as the eigenvectors in Eq. (II.59) for the analogous calculation in the static case. The dominant Floquet doublet condition of Eq. (III.62) requires the Hamiltonian to have two Floquet states which are close to an equal superposition of the $|\text{in}\rangle$ and $|\text{out}\rangle$ states (on average over a time period), but this time with an ω-periodic phase between $|\text{in}\rangle$ and $|\text{out}\rangle$. This ω-periodic phase reflects the ω-periodicity of the Hamiltonian, while the $|\text{in}\rangle$ and $|\text{out}\rangle$ superposition structure is reminiscent of the dominant doublet and ensures that these two Floquet states dominate in the transfer probability expansion of Eq. (III.66).

It is interesting to note that the static dominant doublet condition, with centrosymmetry also imposed, required the existence of *two* eigenvectors independently (Eq. (II.55)). With Floquet-antisymmetry imposed, however, the DFD condition imposes only *one* independent condition on the Floquet states (Eq. (III.72)). Nevertheless, it must be noted that the associated anti-centrosymmetry imposes more constraints on the Hamiltonian than centrosymmetry, because all the elements on the secondary diagonal of an anti-centrosymmetric matrix need to be zero by construction.

IV.1.4 Relevance of transfer times

In the context of fast and efficient energy transport between an input and output site through an intermediate *network* of sites, it is vital that the transport speed and efficiency through the network is not worse than that which would occur in the absence of an intermediate network.

If the transport which would occur due to only direct coupling between the input and output sites were indeed to be on average both faster and more efficient than that assisted by an intermediate network, then the network could be considered redundant. The transfer probability between the sites of a two-site network has been shown to always reach 1 when the sites either have equal on-site energies in the static case [3] or when the energy difference is bridged by vibrational couplings at exact resonance [4]. Therefore, transport between $|\text{in}\rangle$ and $|\text{out}\rangle$ in the absence of a network is always at least as good as that in the presence of a network, in the sense of efficiency, i.e. maximum transfer probability. This means that for the network-assisted transport to improve upon the direct transport, it should occur at faster timescales.

For both the static Hamiltonian studied in [3] and the time-periodic Hamiltonian studied in this thesis, a similar distribution of transfer times for N-site Hamiltonians satisfying the respective design principles was found. In both cases, the mean transfer time was very slightly shorter than that of the corresponding two-site systems, with a significant number of realisations exhibiting transfer times over five times faster than their corresponding two-site systems. This shows that networks can indeed positively assist the transport between an input and output site by speeding up the transfer time.

However, it must be noted that the reference transfer time, i.e. that of the corresponding two-site system, arises from two different parameters in the two cases. For the static case, the reference transfer time is proportional to $1/V$, where $V \equiv V_{1N}$ is the direct input-to-output coupling. In the time-periodic case, the reference transfer time is proportional to $1/2c$, where $2c$ is the direct input-to-output vibrational coupling. Given the initial assumption that the vibrational couplings are smaller than the static ones, this is tantamount to saying that transport occurs slower in the vibrating case than in the static one, given equal parameters for the static couplings. Whether the timescale of transport under the time-periodic Hamiltonian is fast enough with respect to typical decoherence times in a network can only be calculated when precise values of the vibrational couplings are known. For present applications, such as the FMO complex, this requires further experimental data in addition to a theoretical model explicitly involving decoherence.

In [3], an analytical expression was derived for the distribution of transfer times for the static Hamiltonian, which was shown to be consistent with the numerical simulations. In this thesis, the statistics of transfer times were only investigated numerically for illustration purposes, with the main focus of the thesis being the design principles. In order to bring the results of transfer times to the same rigour as those for the design principles, a path for future work could be to derive an analytic expression for the full distribution of transfer times under time-periodic Hamiltonians satisfying the dominant Floquet doublet condition.

IV.2 Biological application to the FMO complex

Returning back to the original motivation for this work, namely energy transport in the FMO complex, a few points can be made on the contribution of the present work to this topic. In Chapter I, the characteristics of the theoretical approach taken in this thesis were outlined, namely building a statistical model with minimal ingredients and looking for design principles that enhance transport. The foundation of this model was laid in [1] but this included neither the energy gradient of the on-site energies nor coupling to the environment. With the extended model presented in this thesis, the three features of static couplings, an on-site energy gradient and coupling to external vibrations are considered. The FMO complex exhibits far more degrees of freedom than can be considered in any tractable theoretical model, so the dominant degrees of freedom must be singled out and all others neglected. Exactly which degrees of freedom can be considered dominant is a matter of debate. Given the current literature on this topic discussed in Chapter I, it is however plausible to assume that the three features included in the model considered in this thesis indeed dominate in the transport process.

Under this assumption, the results of this thesis show that, in principle, it is possible to design a statistical ensemble of networks for energy transport, consistent with the known structure of the FMO wire, in which efficient *quantum* transport, despite statistical variations, is ensured in each realisation. Whether such a design is implemented in nature is a matter for future experiments to find out. How design principles such as Floquet-antisymmetry and the dominant Floquet doublet would be implemented by a biological system are also unanswered questions. Physically, (anti-)centrosymmetry could potentially be implemented by building the structure of the FMO wire such that it is symmetric about its centre. Conditions on the eigenvectors such as the dominant (Floquet) doublet are however more difficult to understand physically and it is not so clear how a biological system could directly implement such a design principle. Here, the statistical investigations come into play. Centrosymmetry greatly increases the probability of obtaining a dominant doublet and Floquet-antisymmetry greatly increases the probability of obtaining a dominant Floquet doublet. Hence, if the relevant symmetry properties *can* be directly imposed as physical design principles in the biological system, then a significant proportion of realisations will exhibit the high efficiency characteristics associated with dominant (Floquet) doublet realisations.

An important extension to the model that is recommended as a next step for further research is explicitly including couplings of the FMO network to the antenna complex and reaction centre at the input and output sites, respectively. Recent experimental data presented in [29] suggests a clear separation of timescales between transport within the FMO wire (0.1–20 ps) and transport from the antenna to the wire and wire to the reaction centre (17 ps and 70 ps, respectively). This suggests that quantum coherences are unlikely to be present in transport between the different parts of the light-harvesting complex, despite potentially playing an

important role within the FMO wire itself. With a model in place that takes into account the full process of energy transfer from capturing the photon in the antenna to delivering the energy to the reaction centre, potential functional effects arising from quantum coherent transport in the FMO wire can be identified.

IV.3 Conclusion

The aim of this thesis was to generalise the design principles found in [3] for efficient quantum transport in disordered networks to the case of a network with an on-site energy gradient and coupling to an external vibrational mode, described by a time-periodic Hamiltonian. The first design principle, namely centrosymmetry of the Hamiltonian, was replaced with a compound symmetry in space and time, named *Floquet-antisymmetry*. This new symmetry was shown to increase the probability of obtaining a Hamiltonian realisation exhibiting efficient transport. To understand why this might be the case, transport under a general 3×3 Hamiltonian satisfying Floquet-antisymmetry was calculated analytically using Floquet and perturbation theory methods. Such a Hamiltonian was found to exhibit a maximum transfer probability close to unity. The desirable properties of the *Floquet states* of this Hamiltonian were used to formulate the *dominant Floquet doublet* condition, analogous to the dominant doublet design principle of the original model. Finally, statistical simulations of Hamiltonians satisfying the two design principles were carried out, showing that intermediate sites can greatly speed up transport. A discussion of the results identified their physical significance as well as potential applications to the FMO complex and other fields. Some suggestions for further research were presented, in particular on investigating the effect of coupling the input and output sites to external channels, through which the excitation is received and released from the network.

Overall, the results of this thesis have shown that energy transport in quantum networks subject to the effects of external oscillations and statistical disorder variations can be optimised in both speed and efficiency by imposing two general design principles on the structure of the network. These principles of network design could be used to understand potential quantum effects in the FMO photosynthetic complex, and may in addition prove useful in the design of networks in other fields such as artificial light-harvesting and quantum information.

Appendix

Derivation of exact dominant Floquet doublet bound

In this Appendix, the exact bound for the maximum transfer probability for time-periodic Hamiltonians satisfying the dominant Floquet doublet condition of Eq. (III.62) is derived. From Eq. (III.68), the bound for the transfer probability under such a Hamiltonian is given by

$$\begin{aligned}\mathscr{P}(t=t_0+kT) \geq \Bigg| &\frac{i}{2}e^{-i\varepsilon_+ kT}\frac{1}{T}\int_0^T |\langle +(t_0)|\phi_+(t_0)\rangle|^2\,\mathrm{d}t_0 - \frac{i}{2}e^{-i\varepsilon_- kT}\frac{1}{T}\int_0^T |\langle -(t_0)|\phi_-(t_0)\rangle|^2\,\mathrm{d}t_0 \\ &+ \sum_{\substack{i=1\\ i\neq +}}^{N}\frac{i}{2}e^{-i\varepsilon_i kT}\frac{1}{T}\int_0^T |\langle +(t_0)|\phi_i(t_0)\rangle|^2\,\mathrm{d}t_0 - \sum_{\substack{i=1\\ i\neq -}}^{N}\frac{i}{2}e^{-i\varepsilon_i kT}\frac{1}{T}\int_0^T |\langle -(t_0)|\phi_i(t_0)\rangle|^2\,\mathrm{d}t_0 \\ &+ \sum_{i=1}^{N} e^{-i\varepsilon_i kT}\frac{1}{T}\int_0^T \Re\Big[\,\langle +(t_0)|\phi_i(t_0)\rangle\langle\phi_i(t_0)|-(t_0)\rangle\,\Big]\,\mathrm{d}t_0\Bigg|^2.\end{aligned} \tag{III.68}$$

The three sums on the right-hand side of this inequality are small and a bound for their maximum contribution can be derived. To this end, consider the orthonormality of the $|\pm(t)\rangle$ states from Eq. (III.60). Integrating over this orthonormality relation and inserting the completeness relation of the Floquet states at every time t from Eq. (II.20) [7]:

$$\begin{aligned}1 &= \frac{1}{T}\int_0^T \langle\pm(t_0)|\pm(t_0)\rangle\,\mathrm{d}t_0 \\ &= \frac{1}{T}\int_0^T \sum_{i=1}^{N}\langle\pm(t_0)|\phi_i(t_0)\rangle\langle\phi_i(t_0)|\pm(t_0)\rangle\,\mathrm{d}t_0 \\ &= \frac{1}{T}\int_0^T \sum_{i=1}^{N}\big|\langle\pm(t_0)|\phi_i(t_0)\rangle\big|^2\,\mathrm{d}t_0 \\ \Rightarrow \frac{1}{T}\int_0^T \sum_{i\neq +}^{N}\big|\langle +(t_0)|\phi_i(t_0)\rangle\big|^2\,\mathrm{d}t_0 &= 1-\frac{1}{T}\int_0^T \big|\langle +(t_0)|\phi_+(t_0)\rangle\big|^2\,\mathrm{d}t_0 \leq 1-\beta, \\ \frac{1}{T}\int_0^T \sum_{i\neq -}^{N}\big|\langle -(t_0)|\phi_i(t_0)\rangle\big|^2\,\mathrm{d}t_0 &= 1-\frac{1}{T}\int_0^T \big|\langle -(t_0)|\phi_-(t_0)\rangle\big|^2\,\mathrm{d}t_0 \leq 1-\beta.\end{aligned} \tag{A.1}$$

When this condition is imposed on the first two sums, taking into account the extreme case where all the exponential terms are ± 1, each sum is bounded by

$$\begin{aligned}\frac{1}{2}\left|\sum_{\substack{i=1\\ i\neq +}}^{N} ie^{-i\varepsilon_i kT}\frac{1}{T}\int_0^T |\langle +(t_0)|\phi_i(t_0)\rangle|^2\,\mathrm{d}t_0\right| &\leq \frac{1-\beta}{2},\\ \frac{1}{2}\left|\sum_{\substack{i=1\\ i\neq -}}^{N} ie^{-i\varepsilon_i kT}\frac{1}{T}\int_0^T |\langle -(t_0)|\phi_i(t_0)\rangle|^2\,\mathrm{d}t_0\right| &\leq \frac{1-\beta}{2}.\end{aligned} \tag{A.2}$$

The last sum is more difficult to deal with. Applying the Cauchy-Schwarz inequality to each integral in the last sum,

$$\begin{aligned}\left|\frac{1}{T}\int_0^T \Re\Big[\,\langle +(t_0)|\phi_i(t_0)\rangle\langle\phi_i(t_0)|-(t_0)\rangle\,\Big]\,\mathrm{d}t_0\right| &\leq \frac{1}{T}\int_0^T \Big|\,\langle +(t_0)|\phi_i(t_0)\rangle\langle\phi_i(t_0)|-(t_0)\rangle\,\Big|\,\mathrm{d}t_0\\ &\leq \left(\frac{1}{T}\int_0^T \Big|\,\langle +(t_0)|\phi_i(t_0)\rangle\,\Big|^2\,\mathrm{d}t_0\right)^{\frac{1}{2}}\left(\frac{1}{T}\int_0^T \Big|\,\langle\phi_i(t_0)|-(t_0)\rangle\,\Big|^2\,\mathrm{d}t_0\right)^{\frac{1}{2}}.\end{aligned} \tag{A.3}$$

Applying this result to the $i=\pm$ terms in the last sum, the upper bounds

$$\begin{aligned}&\left|\frac{1}{T}\int_0^T \Re\Big[\,\langle +(t_0)|\phi_+(t_0)\rangle\langle\phi_+(t_0)|-(t_0)\rangle\,\Big]\,\mathrm{d}t_0\right|\\ &\qquad\leq \underbrace{\left(\frac{1}{T}\int_0^T \Big|\,\langle +(t_0)|\phi_+(t_0)\rangle\,\Big|^2\,\mathrm{d}t_0\right)^{\frac{1}{2}}}_{\leq 1}\underbrace{\left(\frac{1}{T}\int_0^T \Big|\,\langle\phi_+(t_0)|-(t_0)\rangle\,\Big|^2\,\mathrm{d}t_0\right)^{\frac{1}{2}}}_{\leq\sqrt{1-\beta}}\leq\sqrt{1-\beta},\\ &\left|\frac{1}{T}\int_0^T \Re\Big[\,\langle +(t_0)|\phi_-(t_0)\rangle\langle\phi_-(t_0)|-(t_0)\rangle\,\Big]\,\mathrm{d}t_0\right|\\ &\qquad\leq \underbrace{\left(\frac{1}{T}\int_0^T \Big|\,\langle +(t_0)|\phi_-(t_0)\rangle\,\Big|^2\,\mathrm{d}t_0\right)^{\frac{1}{2}}}_{\leq\sqrt{1-\beta}}\underbrace{\left(\frac{1}{T}\int_0^T \Big|\,\langle\phi_-(t_0)|-(t_0)\rangle\,\Big|^2\,\mathrm{d}t_0\right)^{\frac{1}{2}}}_{\leq 1}\leq\sqrt{1-\beta},\end{aligned} \tag{A.4}$$

for each of the two terms are obtained [7].

For the rest of the terms in the last sum, the following result is required [7]: Let a_i, b_i be positive real numbers such that $0\leq a_i\leq 1$, $0\leq b_i\leq 1$, $0\leq i\leq M$, $M\in\mathbb{N}$ and

$$\sum_{i=1}^{M} a_i\leq B,\ \sum_{i=1}^{M} b_i\leq B,\ B\in\mathbb{R}. \tag{A.5}$$

Then it can be seen that

$$\sum_{i=1}^{M}\sqrt{a_i}\leq\sqrt{MB}\text{ and }\sqrt{b_i}\leq\sqrt{B},\ \forall i\in\{i\in\mathbb{N}:1\leq i\leq M\}. \tag{A.6}$$

Therefore,

$$\sum_{i=1}^{M}\sqrt{a_i b_i} \le \sqrt{B}\sum_{i=1}^{M}\sqrt{a_i} \le \sqrt{MB}. \tag{A.7}$$

Setting $B = 1-\beta$, $M = N-2$, together with

$$a_i = \frac{1}{T}\int_0^T \Big|\langle +(t_0)|\phi_i(t_0)\rangle\Big|^2 \mathrm{d}t_0, \quad b_i = \frac{1}{T}\int_0^T \Big|\langle \phi_i(t_0)|-(t_0)\rangle\Big|^2 \mathrm{d}t_0, \tag{A.8}$$

an upper bound for the remaining terms in the last sum is obtained:

$$\begin{aligned}
&\left|\sum_{i\neq\pm}^{N} e^{-i\varepsilon_i kT}\frac{1}{T}\int_0^T \Re\Big[\,\langle +(t_0)|\phi_i(t_0)\rangle\,\langle\phi_i(t_0)|-(t_0)\rangle\,\Big]\,\mathrm{d}t_0\right| \\
&\qquad \le \sum_{i\neq\pm}^{N}\left(\frac{1}{T}\int_0^T \Big|\langle +(t_0)|\phi_i(t_0)\rangle\Big|^2 \mathrm{d}t_0\right)^{\frac{1}{2}}\left(\frac{1}{T}\int_0^T \Big|\langle \phi_i(t_0)|-(t_0)\rangle\Big|^2 \mathrm{d}t_0\right)^{\frac{1}{2}} \\
&\qquad \le \sqrt{N-2}\,\big(1-\beta\big).
\end{aligned} \tag{A.9}$$

The upper and lower bounds for the various terms on the right-hand side Eq. (III.68) can now be combined to give a lower bound for the maximum value of the full expression of the right-hand side. The maximum occurs when the exponential factors of the two large terms align in such a way that they add up with a total lower bound of $\beta/2+\beta/2=\beta$. The minimum value that this maximum could take occurs when all the exponential terms in the last three sums align in such a way that each sum takes its greatest possible absolute value with a sign opposite to that of the large terms. Then the minimum value of the maximum (assuming an arbitrarily large reference time T_{R}) is $|\beta-(1-\beta)-2\sqrt{1-\beta}-\sqrt{N-2}\,(1-\beta)|^2$. Therefore,

$$\mathscr{P}_{\max} \ge \max_{t\in[t_0,t_0+T_{\mathrm{R}})} \mathscr{P}(t=t_0+kT) \ge \left|\beta-\Big(1+\sqrt{N-2}\Big)(1-\beta)-2\sqrt{1-\beta}\right|^2, \tag{A.10}$$

which can be made close to one for a sufficiently large choice of β, given a number of sites N of the order of ten.

Acknowledgements

I would like to thank my supervisors Andreas Buchleitner, Gabriel Dufour and Christian Scheppach for their continual advice and support during the research project and for their detailed comments on the first drafts of this thesis. I acknowledge fruitful discussions with Mattia Walschaers and Jonathan Brugger, who previously worked on the topics of this thesis, through which inspirations for many ideas were developed. I am indebted to Josh Hemmerich for much of the thesis layout in LaTeX. I would further like to thank all the other members of the QOS group for welcoming me into the research group and introducing me to life in academic research. Special mention goes to Vyacheslav Shatokhin (Slava) for being an inspirational friend and mentor in life both inside and outside of physics. Moreover, I would like to thank all the friends that I have made in Freiburg over the last year for making my Erasmus year abroad as enjoyable as it was, in particular my flatmates in Händelwohnheim as well as fellow Erasmus physics students Aliya Ismailova, Chris Olley and Adrien Partier. At Imperial, I would like to thank Florian Mintert and Ingo Mueller-Wodarg for all their help and advice concerning the year abroad. Finally, I would like to thank my parents for their invaluable support throughout my studies.

References

[1] M. Walschaers, J. F.-d.-C. Diaz, R. Mulet, and A. Buchleitner, "Optimally designed quantum transport across disordered networks," *Physical Review Letters*, vol. 111, no. 18, p. 180601, 2013.

[2] M. Walschaers, R. Mulet, T. Wellens, and A. Buchleitner, "Statistical theory of designed quantum transport across disordered networks," *Physical Review E*, vol. 91, no. 4, p. 042137, 2015.

[3] M. Walschaers, *Efficient quantum transport* (PhD thesis). Albert-Ludwigs-Universität Freiburg, KU Leuven, 2016.

[4] J. Brugger, *Phononen-assistierter Quantentransport auf endlichen Netzwerken* (Bachelor's thesis). Albert-Ludwigs-Universität Freiburg, 2015.

[5] G. S. Engel, T. R. Calhoun, E. L. Read, T.-K. Ahn, T. Mancal, Y.-C. Cheng, R. E. Blankenship, and G. R. Fleming, "Evidence for wavelike energy transfer through quantum coherence in photosynthetic systems," *Nature*, vol. 446, no. 7137, pp. 782–786, 2007.

[6] J. H. Shirley, *Interaction of a quantum system with a strong oscillating field* (PhD thesis). California Institute of Technology, 1963.

[7] J. Brugger. Personal communication, December 2016.

[8] R. E. Blankenship, *Molecular mechanisms of photosynthesis*. Blackwell Science, Oxford, 2002.

[9] G. D. Scholes, G. R. Fleming, L. X. Chen, A. Aspuru-Guzik, A. Buchleitner, D. F. Coker, G. S. Engel, R. van Grondelle, A. Ishizaki, D. M. Jonas, J. S. Lundeen, J. K. McCusker, S. Mukamel, J. P. Ogilvie, A. Olaya-Castro, M. A. Ratner, F. C. Spano, K. B. Whaley, and X. Zhu, "Using coherence to enhance function in chemical and biophysical systems," *Nature*, vol. 543, no. 7647, pp. 647–656, 2017.

[10] N. Lambert, Y.-N. Chen, Y.-C. Cheng, C.-M. Li, G.-Y. Chen, and F. Nori, "Quantum biology," *Nature Physics*, vol. 9, no. 1, pp. 10–18, 2013.

[11] N. Christensson, H. F. Kauffmann, T. Pullerits, and T. Mančal, "Origin of long-lived coherences in light-harvesting complexes," *The Journal of Physical Chemistry B*, vol. 116, no. 25, pp. 7449–7454, 2012.

[12] H.-G. Duan, V. I. Prokhorenko, R. Cogdell, K. Ashraf, A. L. Stevens, M. Thorwart, and R. J. D. Miller, "Nature does not rely on long-lived electronic quantum coherence for photosynthetic energy transfer," *arXiv:1610.08425* [physics.bio-ph], 2016.

[13] A. Ishizaki and G. R. Fleming, "Theoretical examination of quantum coherence in a photosynthetic system at physiological temperature," *Proceedings of the National Academy of Sciences*, vol. 106, no. 41, pp. 17255–17260, 2009.

[14] D. M. Wilkins and N. S. Dattani, "Why quantum coherence is not important in the Fenna-Matthews-Olsen complex," *Journal of Chemical Theory and Computation*, vol. 11, no. 7, pp. 3411–3419, 2015.

[15] M. Schmidt am Busch, F. Müh, M. El-Amine Madjet, and T. Renger, "The eighth bacteriochlorophyll completes the excitation energy funnel in the FMO protein," *The Journal of Physical Chemistry Letters*, vol. 2, no. 2, pp. 93–98, 2011.

[16] T. Mančál, N. Christensson, V. Lukeš, F. Milota, O. Bixner, H. F. Kauffmann, and J. Hauer, "System-dependent signatures of electronic and vibrational coherences in electronic two-dimensional spectra," *The Journal of Physical Chemistry Letters*, vol. 3, no. 11, pp. 1497–1502, 2012.

[17] J. H. Shirley, "Solution of the Schrödinger equation with a Hamiltonian periodic in time," *Physical Review*, vol. 138, no. 4B, pp. B979–B987, 1965.

[18] S. Sauer, *Entanglement in periodically driven quantum systems* (PhD Thesis). Albert-Ludwigs-Universität Freiburg, 2013.

[19] M. Grifoni and P. Hänggi, "Driven quantum tunneling," *Physics Reports*, vol. 304, pp. 229–354, 1998.

[20] Y. A. Zel'dovich, "The quasienergy of a quantum-mechanical system subjected to a periodic action," *Soviet Physics JETP*, vol. 24, no. 5, pp. 1006–1008, 1967.

[21] C. Cohen-Tannoudji, B. Diu, and F. Laloë, *Quantum mechanics*. Wiley, 1977.

[22] M. Reed and B. Simon, *Methods of modern mathematical physics, vol. I: functional analysis*. Academic Press, 1980.

[23] T. Zech, R. Mulet, T. Wellens, and A. Buchleitner, "Centrosymmetry enhances quantum transport in disordered molecular networks," *New Journal of Physics*, vol. 16, no. 5, p. 055002, 2014.

[24] I. T. Abu-Jeib, "Centrosymmetric matrices: properties and an alternative approach," *Canadian Applied Mathematics Quarterly*, vol. 10, no. 4, pp. 429–445, 2002.

[25] V. B. Berestetskii, E. M. Lifshitz, and L. P. Pitaevskii, *Landau and Lifshitz course of theoretical physics, vol. 4: quantum electrodynamics* (2nd ed.). Elsevier, 1982.

[26] H. V. McIntosh, *Linear algebra* (lecture notes). Universidad Autónoma de Puebla, 2004.

[27] M. A. Nielsen and I. L. Chuang, *Quantum computation and quantum information*. Cambridge University Press, 2000.

[28] H. Anton, *Elementary linear algebra*. John Wiley and Sons, 1994.

[29] J. Dostál, J. Pšenčík, and D. Zigmantas, "In situ mapping of the energy flow through the entire photosynthetic apparatus," *Nature Chemistry*, vol. 8, no. 7, pp. 705–710, 2016.